

5858  
NACA TN 2160

0065103



TECH LIBRARY KAFB, NM

# NATIONAL ADVISORY COMMITTEE FOR AERONAUTICS

TECHNICAL NOTE 2160

MEASUREMENTS OF SECTION CHARACTERISTICS OF A  $45^\circ$  SWEPT WING  
SPANNING A RECTANGULAR LOW-SPEED WIND TUNNEL AS  
AFFECTED BY THE TUNNEL WALLS

By Robert E. Dannenberg

Ames Aeronautical Laboratory  
Moffett Field, Calif.



Washington

August 1950

AFMAG  
TECHNICAL NOTE  
AFL 2011

819-70/41



## NATIONAL ADVISORY COMMITTEE FOR AERONAUTICS

## TECHNICAL NOTE 2160

MEASUREMENTS OF SECTION CHARACTERISTICS OF A  $45^\circ$  SWEEP WING

## SPANNING A RECTANGULAR LOW-SPEED WIND TUNNEL AS

## AFFECTED BY THE TUNNEL WALLS

By Robert E. Dannenberg

## SUMMARY

An investigation was conducted to determine the efficacy of simulating the flow over a swept wing of infinite span by mounting a swept wing across the test section of a closed rectangular wind tunnel. Two constant-chord wings were tested; one unswept and the other swept  $45^\circ$ . The sections perpendicular to the leading edge were the NACA 63<sub>1</sub>-012. The angle of attack was varied from  $0^\circ$  to the stall for the unswept wing and from  $0^\circ$  to  $12^\circ$  for the swept wing.

Equations are presented from which the upwash velocities induced by the tunnel walls were calculated for the swept wing. Corrections to the angle of attack of the swept wing were applied according to the calculated induced velocities.

The experimental results indicate that the change in the pressure distribution and in the lift characteristics over the central half of the swept wing compared to that over the unswept wing was in accordance with simple sweep theory. The differences in the wake drag and in the moment characteristics were small.

## INTRODUCTION

The chordwise distribution of pressure over a yawed wing of infinite span and constant chord in a potential flow field is invariant along the span. The investigations of references 1 and 2 have indicated that the characteristics of a section at the center of a constant-chord wing mounted across a wind tunnel obliquely to the free-stream direction are essentially those of an infinite span wing; however, the pressure measurements verifying this similarity were made only at the center of the span of the wing where the interference of the tunnel walls is small and did not include measurements of the spanwise variation of pressure. Should experiment show that the effects of sweep are uniform over a reasonable portion of the span, a wing mounted in this manner could be used for evaluating the

changes in pressure distribution over a swept wing caused, for instance, by the addition of a nacelle or a leading-edge inlet.

An experimental investigation was undertaken in one of the Ames 7-by 10-foot wind tunnels to study, by means of pressure-distribution and wake measurements, the flow over a constant-chord  $45^\circ$  swept wing that completely spanned the wind tunnel. To ascertain the portion of the span for which the flow satisfactorily approximates the flow about a yawed wing of infinite span, the section characteristics of the swept wing are compared with those of an unswept wing having the same airfoil section perpendicular to the leading edge. The basic comparison is between the chordwise distributions of pressure, at various distances from the tunnel walls, for the swept wing with distributions for the unswept wing. The data for the unswept wing were corrected to free-air conditions by the method discussed in reference 3. The data for the swept wing were corrected for the effects of the tunnel walls on the induced upwash velocities at the wing quarter-chord line. Equations for the swept-wing corrections were developed by Mr. John DeYoung of the Ames Laboratory and are included in the appendix.

#### COEFFICIENTS AND SYMBOLS

The following coefficients and symbols are used in this report:

$c$	chord of wing parallel to flow direction
$c_d$	wake drag coefficient
$c_l$	section lift coefficient
$c_{m_{c/4}}$	section pitching-moment coefficient about the quarter-chord point
$P$	pressure coefficient $\left( \frac{p_l - p_o}{q_o} \right)$
$p$	static pressure
$q$	dynamic pressure
$V$	velocity
$\alpha$	angle of attack in streamwise plane, degrees

The following subscripts are used in conjunction with the above coefficients and symbols:

l        local  
o        free stream  
u        uncorrected

#### MODEL AND APPARATUS

The unswept wing was mounted vertically in the wind tunnel as shown in figure 1. The swept wing was mounted horizontally. (See fig. 2.) The sections perpendicular to the leading edge of both wings were the NACA 63<sub>1</sub>-012. Coordinates for the NACA 63<sub>1</sub>-012 section are given in reference 4. The unswept wing had a chord of 4 feet; whereas the swept wing had a chord of 2.5 feet perpendicular to the leading edge. The axis of rotation for angle-of-attack changes of the unswept wing was the one-quarter-chord line; whereas that for the swept wing crossed the midspan station at 35 percent of the chord and was horizontal and perpendicular to the stream direction as shown in figure 3.

The pressure distribution over the swept wing was measured by orifices in the surface of the model that were connected to multiple-tube manometers. The swept wing had rows of pressure orifices in the stream direction at the 27.5-, 50-, and 72.5-percent-span stations. (See fig. 3.) Additional orifices were located along constant-chord lines at 5, 15, 30, 50, and 80 percent of the chord. The chordwise distribution of pressure over the unswept wing was measured by a row of orifices at the center of the span.

The wake pressures used in calculation of the drags of the wings were measured by a survey rake that was connected to an integrating manometer. The location of the survey planes behind the swept wing is indicated in figure 3. For the unswept wing, the rake was approximately one-half-chord length behind the trailing edge.

#### TESTS

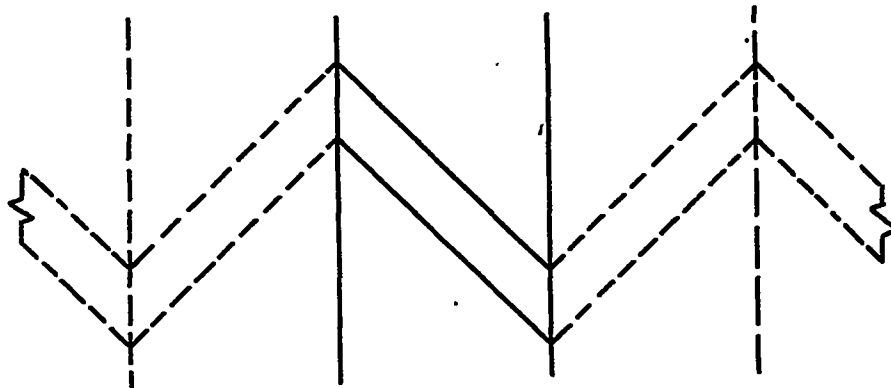
For the unswept wing, measurements of the surface pressures for angles of attack from 0° to 12° were made at a test Mach number of 0.14. The Reynolds number was 3,840,000 based on the chord. Tunnel-wall corrections to the angle of attack and section lift coefficient of this wing were applied according to the methods discussed in reference 3 by the following equations:

$$\alpha = \alpha_u + 0.303 c_{l_u}$$

$$c_l = 0.953 c_{l_u}$$

For the swept wing, measurements of the surface pressures at angles of attack from  $0^\circ$  to  $12^\circ$  were made at a test Mach number of 0.16. The Reynolds number was 3,900,000 based on the chord in the stream direction. In addition, wake-drag measurements were made for various test Reynolds numbers up to 8,100,000.

Tunnel-wall corrections for the swept wing are presented in the appendix. In the derivation of the corrections, the swept wing was considered to correspond to a panel of a kinked wing as shown in the following sketch, the tunnel walls functioning as reflection planes:



Tunnel-wall corrections to the angle of attack were applied according to the equation

$$\alpha = \alpha_u + \frac{k_1 c_l}{1 + k_2 c_l}$$

Values of  $k_1$  and  $k_2$  for the swept wing of this investigation are presented in the appendix. The correction to the angle of attack was found by calculation to vary along the span as noted in the following table:

Station (percent)	$\alpha$ corrected, deg		
	$\alpha_u, 4^\circ$	$\alpha_u, 8^\circ$	$\alpha_u, 12^\circ$
27.5	4.02	8.04	12.07
50	4.14	8.29	12.41
72.5	4.32	8.58	12.76

## RESULTS AND DISCUSSION

## Pressure Distribution

The pressure distribution over the center section of the unswept wing is shown in figure 4. For the swept wing, the chordwise distributions of pressure over the upper surface at the 27.5-, 50-, and 72.5-percent-span stations are shown in figure 5. The corresponding distributions over the lower surface are given in figure 6. For the swept wing, the spanwise distributions of pressure along the 5-, 15-, 30-, 50-, and 80-percent-chord lines are shown in figure 7. Inspection of figure 7 reveals that the influence of the tunnel walls is greatest near the leading edge and at the higher angles of attack, is opposite in sense at the two walls, and diminishes with increasing distance from each wall so that a region of substantially uniform flow results over approximately the center half of the span. From the figure a determination may be made of the region in which the flow is sufficiently uniform for any particular use.

The disturbance engendered by the vertical walls possibly may be decreased by distorting the walls to conform to the streamline pattern of the flow as indicated in reference 5. The walls were not distorted for the tests reported herein.

Simple sweep considerations indicate that pressure coefficients for a swept wing of infinite aspect ratio should vary as the square of the cosine of the angle of sweep. For a sweep of  $45^\circ$ , the stagnation pressure coefficient should then be 0.50 instead of 1.0 in incompressible flow. The results are in close agreement with this value. In figure 8(a), the measured pressure distribution over the swept wing and the distribution computed by multiplying the measured pressure coefficients for the unswept wing by the factor  $\cos^2 45^\circ$  are compared at zero lift. As shown in the figure, the agreement is excellent. Only the comparison at the midspan station is presented, as the agreements at the 27.5- and 72.5-percent-span stations were equally close.

In figures 8(b), 8(c), and 8(d), the measured and computed pressure distributions at the midspan station are compared for angles of attack of  $2.1^\circ$ ,  $5^\circ$ , and  $7.5^\circ$ . The corresponding angles of attack of the unswept wing were determined from the relation

$$\alpha_{\text{swept wing}} = \alpha_{\text{unswept wing}} \times \cos 45^\circ$$

The agreement of the computed values with the measured values is good within the angle-of-attack range of this investigation, indicating satisfactory agreement with simple sweep theory for the swept wing pitched about a lateral axis.

### Force and Moment Characteristics

The variation of section lift coefficient along the span of the swept wing is shown in figure 9 for both corrected and uncorrected angles of attack. The lift coefficients were obtained by integration of chordwise pressure-distribution diagrams. At the 27.5-, 50-, and 72.5-percent-span stations there were a large number of pressure orifices which clearly defined the shape of the pressure diagrams. At other stations there were only five orifices on the upper surface and five orifices on the lower surface. For the stations with the fewer orifices, the shape of the diagrams was determined by fairing a curve through the five experimental points, using as a guide the shape of the pressure distribution at the closest of the three stations previously mentioned.

Inspection of figure 9 shows that the section lift coefficient increased slightly between 27.5 and 72.5 percent of the span for constant values of the corrected angle of attack. The variation of section lift coefficient with angle of attack is shown in figure 10(a) for the 27.5-, 50-, and 72.5-percent-span stations. For angles of attack greater than  $11^\circ$ , a decrease in lift-curve slope occurred at the latter two stations. Inspection of the pressure-distribution diagrams indicates that the extent of the spanwise flow separation was increasing. In figure 10(b), the lift characteristics of the unswept wing are compared to those at the midspan of the swept wing. The maximum lift of the unswept wing occurred at  $13.6^\circ$  angle of attack. Simple sweep considerations indicate that the lift-curve slope of the swept wing should vary as the cosine of the angle of sweep. Included in figure 10(b) is the lift curve of the swept wing computed by multiplying the lift coefficient of the unswept wing by the cosine of  $45^\circ$ . It is seen that computed values are in close agreement with the test results throughout the angle-of-attack range of the investigation.

The pitching-moment characteristics of the swept and of the unswept wing are shown in figure 11. There was no perceptible change in the pitching-moment characteristics about the one-quarter-chord point of a section of the swept wing compared to that of the unswept wing.

The spanwise variation of the wake drag of the swept wing as calculated from the momentum defect in the wake is shown in figure 12. The data shown in the figure would indicate that in the angle-of-attack range from  $0^\circ$  to  $5^\circ$  or  $6^\circ$  the boundary-layer flow had only a slight tendency to build up spanwise along the wing. Above an angle of attack of  $6^\circ$  there was a pronounced increase of the wake drag along the span toward the right wall. In figure 13(a), the variation of the drag coefficient with angle of attack is shown for both the unswept and the swept wing. The variation of the wake drag of the swept wing as a function of the Reynolds number is shown in figure 13(b) for an angle of attack of  $0^\circ$ .

## Air Flow Over the Swept Wing

Tuft studies are presented in figure 14 for angles of attack of  $0^\circ$ ,  $5^\circ$ ,  $8^\circ$ , and  $12^\circ$  to give an idea of the direction and type of flow in the boundary layer of the swept wing. The tuft pictures were taken by two cameras above the model. The heavy dashed line in the pictures was normal to the wing leading edge as shown in figure 3. For an angle of attack of  $5^\circ$ , the flow adjacent to the right wall was unsteady. (See fig. 14(d).) As the angle of attack was increased above  $5^\circ$ , the region of unsteady flow near the right wall became more prominent. The flow over the left side of the wing adjacent to the wall was steady throughout the angle-of-attack range of the investigation.

Inspection of the tuft pictures indicates that the flow adjacent to the surface over the leading edge of the wing turned slightly in the direction of a line normal to the leading edge and was largely independent of changes in the angle of attack. For an angle of attack of  $0^\circ$  (figs. 14(a) and 14(c)), the flow over the rear 30 to 40 percent of the wing was more nearly aligned with the free-stream direction. As the angle of attack was increased, the tufts on the rear portion of the wing turned in a direction more nearly parallel with the trailing edge, indicating more spanwise flow. For an angle of attack of  $12^\circ$  (figs. 14(f) and 14(h)), these tufts were parallel to the trailing edge of the wing. Tufts 0.25 and 0.50 inch above the wing surface, supported by wires normal to the surface, indicated considerably less spanwise flow than did those on the wing surface.

## CONCLUDING REMARKS

The results of this low-speed investigation indicate the practicability of simulating the flow over a swept wing of infinite span throughout a small range of angles of attack with a swept wing that completely spans a closed wind tunnel. The change in the pressure-coefficient distribution and in the lift characteristics over the central half of the span were in accord with calculations based on simple sweep theory. The differences in the wake drag, and particularly in the moment characteristics, of the swept wing compared to the unswept wing were found to be small.

Ames Aeronautical Laboratory,  
National Advisory Committee for Aeronautics,  
Moffett Field, Calif., May 26, 1950.



## APPENDIX

TUNNEL-WALL CORRECTIONS FOR INDUCED UPWASH VELOCITY  
FOR A SWEEP WING OF CONSTANT CHORD COMPLETELY  
SPANNING A RECTANGULAR WIND TUNNEL

In order to compare the test results for the swept wing with those for the unswept wing, it is necessary to consider tunnel-wall interference effects on both wings. Tunnel-wall corrections for the unswept wing were applied according to the methods discussed in reference 3. Analysis of the problem for the swept wing indicates that it is necessary to determine the extent to which the tunnel walls alter the angle of attack from what it would be if the walls were not present. As this discussion is limited to swept wings placed midway between the upper and lower tunnel walls, the correction to the angle of attack is considered to be dependent upon the magnitude of tunnel-wall-induced velocity at the horizontal center plane of the wind tunnel.

The increase in the axial velocity of the flow about the swept wing due to the restraint imposed by the horizontal tunnel walls is believed to be small. For the unswept wing, this increase in the axial velocity resulted in a value 1.007 times the velocity of the undisturbed stream. The maximum cross-section area of the swept wing in planes normal to the stream direction was less than one-sixth that of the unswept wing. Thus, at no position along the span of the swept wing should the increase in axial velocity be as large as that for the unswept wing.

For an infinite yawed wing in potential flow, lines of constant pressure are parallel to the leading edge of the wing. Ideally, the flow over the swept wing of this investigation should correspond to the flow over the yawed wing. However, because the vertical tunnel walls functioned as reflection planes, the wing corresponded more nearly to a panel of a kinked wing, as illustrated in figure 15. In the computation of the tunnel-wall corrections, the lines of constant pressure were considered parallel to the leading edges of the respective wing panels. It was realized that adjacent to the vertical walls, the lines of constant pressure were no longer parallel to the leading edge but were curved and became normal to the walls at the walls. With this discrepancy in flow alignment, the computed corrections were not expected to be adequate adjacent to the vertical walls. The calculated corrections should be satisfactory for correcting to approximately free-air conditions for sections of the wing more than one chord length from either wall.

The correction to the angle of attack for the swept wing was calculated by the method of images in which the wing was represented by a bound vortex along the one-quarter-chord line. The effects of the horizontal tunnel walls were calculated by introducing a three-dimensional lattice of images above and below the wing, the images being alternately inverted,

and direct images of the wing itself. Due to the sweep of the bound vortex, it was necessary to extend the images to the right and left of the side walls of the tunnel as shown in figure 15(a).

By considering each image in turn, an expression was obtained for the induced velocity at the lifting line. As a result of the sweep of the lifting line, the total induced velocity was not normal to the flow direction. The velocity components parallel and normal to the free-stream direction were determined from the equation of the total induced velocity developed by Mr. DeYoung.

The total velocity induced by the image vortex at position  $m, n$  as shown in figure 15(a) is

$$\sqrt{u^2 + v^2 + w^2} = \frac{\Gamma \sec \Lambda}{4\pi a \sqrt{n^2 \sin^2 \Lambda + m^2 \left(\frac{h}{a}\right)^2}} \times \left[ \frac{n \cos^2 \Lambda - \frac{y}{a} + \frac{1}{2}}{\sqrt{\left(\frac{y}{a} - \frac{1}{2}\right)^2 \tan^2 \Lambda + \left(\frac{y}{a} - \frac{1}{2} - n\right)^2 + m^2 \left(\frac{h}{a}\right)^2}} - \frac{n \cos^2 \Lambda - \frac{y}{a} - \frac{1}{2}}{\sqrt{\left(\frac{y}{a} + \frac{1}{2}\right)^2 \tan^2 \Lambda + \left(\frac{y}{a} + \frac{1}{2} - n\right)^2 + m^2 \left(\frac{h}{a}\right)^2}} \right] \quad (1)$$

where

$a$  width of the tunnel

$C$  cross-section area of tunnel

$c_l$  section lift coefficient

$h$  height of the tunnel

$S$  wing area

$u$  component of induced velocity parallel to  $x$  axis

$v$  component of induced velocity parallel to  $y$  axis

$w$  component of induced velocity parallel to  $z$  axis

$y$  distance parallel to  $y$  axis measured from midspan of wing  
(See fig. 15.)

- $\Lambda$  angle of sweep of wing  
 $\Gamma$  circulation strength of vortex  
 $m, n$  integers defining image location (See fig. 15(a).)  
 $k_1, k_2$  interference factors

The components of the total induced velocity parallel and normal to the free-stream direction are

$$\left. \begin{aligned} u &= \sqrt{u^2 + v^2 + w^2} \times \xi \\ v &= \sqrt{u^2 + v^2 + w^2} \times \eta \end{aligned} \right\} \quad (2)$$

where  $\xi$  is the direction cosine of the total induced velocity with respect to the  $x$  axis and  $\eta$  is the direction cosine with respect to the  $y$  axis. The values of the direction cosines are calculated from the equations

$$\left. \begin{aligned} \xi &= \frac{m \left( \frac{h}{a} \right) \cos \Lambda}{\sqrt{n^2 \sin^2 \Lambda + m^2 \left( \frac{h}{a} \right)^2}} \\ \eta &= \frac{-m \left( \frac{h}{a} \right) \sin \Lambda}{\sqrt{n^2 \sin^2 \Lambda + m^2 \left( \frac{h}{a} \right)^2}} \end{aligned} \right\} \quad (3)$$

To simplify the calculation, let

$$K_y(m, n) = \frac{1}{4\pi \left[ n^2 \sin^2 \Lambda + m^2 \left( \frac{h}{a} \right)^2 \right]} \times \left[ \begin{aligned} &\frac{n \cos^2 \Lambda - \frac{y}{a} + \frac{1}{2}}{\sqrt{\left( \frac{y}{a} - \frac{1}{2} \right)^2 \tan^2 \Lambda + \left( \frac{y}{a} - \frac{1}{2} - n \right)^2 + m^2 \left( \frac{h}{a} \right)^2}} \\ &\frac{n \cos^2 \Lambda - \frac{y}{a} - \frac{1}{2}}{\sqrt{\left( \frac{y}{a} + \frac{1}{2} \right)^2 \tan^2 \Lambda + \left( \frac{y}{a} + \frac{1}{2} - n \right)^2 + m^2 \left( \frac{h}{a} \right)^2}} \end{aligned} \right] \quad (4)$$

The upwash velocity per unit circulation is

$$\frac{w}{\Gamma} = \frac{n \tan \Lambda}{a} Ky(m,n) \quad (5)$$

This component of velocity is expressed as a correction to the angle of attack  $\alpha_u$  as

$$\Delta \alpha_1 = \frac{1}{2} \left( \frac{h}{a} \right) \frac{S}{C} \frac{w a}{\Gamma} c_l \times 57.3 = k_1 c_l \quad (6)$$

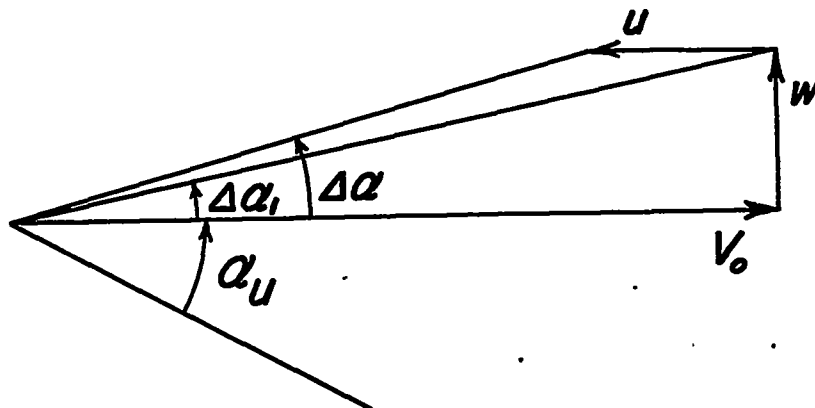
The correction for the induced velocity component in the free-stream direction is

$$u_{c/4} = \frac{\Gamma}{a} \left( m \frac{h}{a} \right) Ky(m,n) \quad (7)$$

and as

$$\begin{aligned} \Gamma &= \frac{1}{2} \left( \frac{S}{C} \right) h V_o c_l \\ \left( \frac{u}{V_o} \right)_{c/4} &= \frac{1}{2} \left( \frac{h}{a} \right)^2 \frac{S}{C} m Ky(m,n) c_l = k_2 c_l \end{aligned} \quad (8)$$

The total correction to the angle of attack is obtained from equations (6) and (8) as indicated in the following velocity-component diagram:



The correction to the angle of attack is

$$\alpha = \alpha_u + \frac{k_1 c_l}{1 + k_2 c_l} \quad (9)$$

The variations of the constants  $k_1$  and  $k_2$  with distance along the span for the  $45^\circ$  swept wing in the 7- by 10-foot wind tunnel are shown in figure 15(c).

#### REFERENCES

1. Göthert, B.: High-Speed Measurements on a Swept-Back Wing (Sweepback Angle  $\phi = 35^\circ$ ). NACA TM 1102, 1947.
2. Lippisch, A., and Beuschausen, W.: Pressure Distribution Measurements at High Speed and Oblique Incidence of Flow. NACA TM 1115, 1947.
3. Allen, H. Julian, and Vincenti, Walter G.: Wall Interference in a Two-Dimensional-Flow Wind Tunnel, with Consideration of the Effect of Compressibility. NACA Rep. 782, 1944.
4. Abbott, Ira M., von Doenhoff, Albert E., and Stivers, Louis S., Jr.: Summary of Airfoil Data. NACA Rep. 824, 1945.
5. Watkins, C.: The Streamline Pattern in the Vicinity of an Oblique Airfoil. NACA TN 1231, 1947.

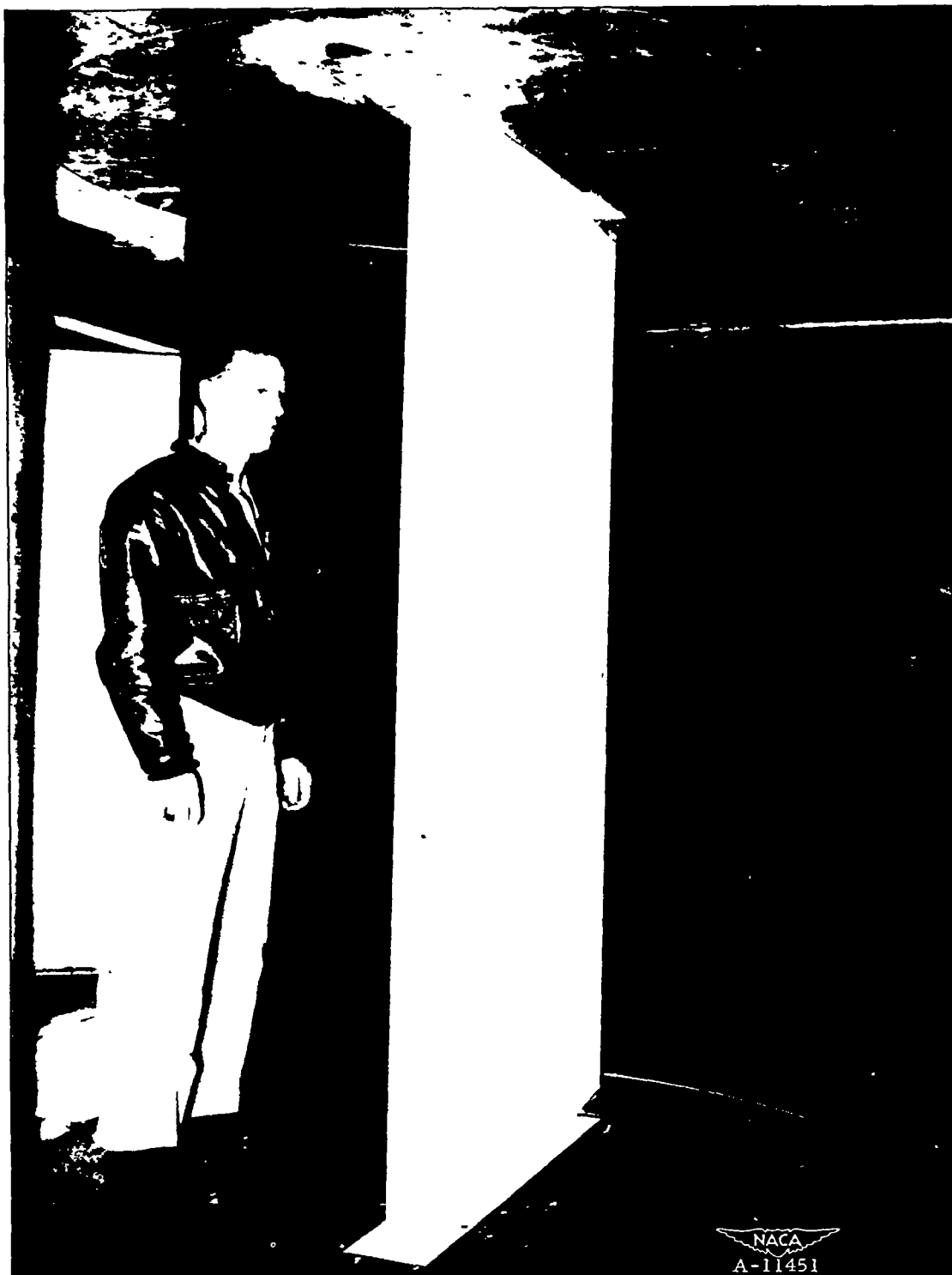
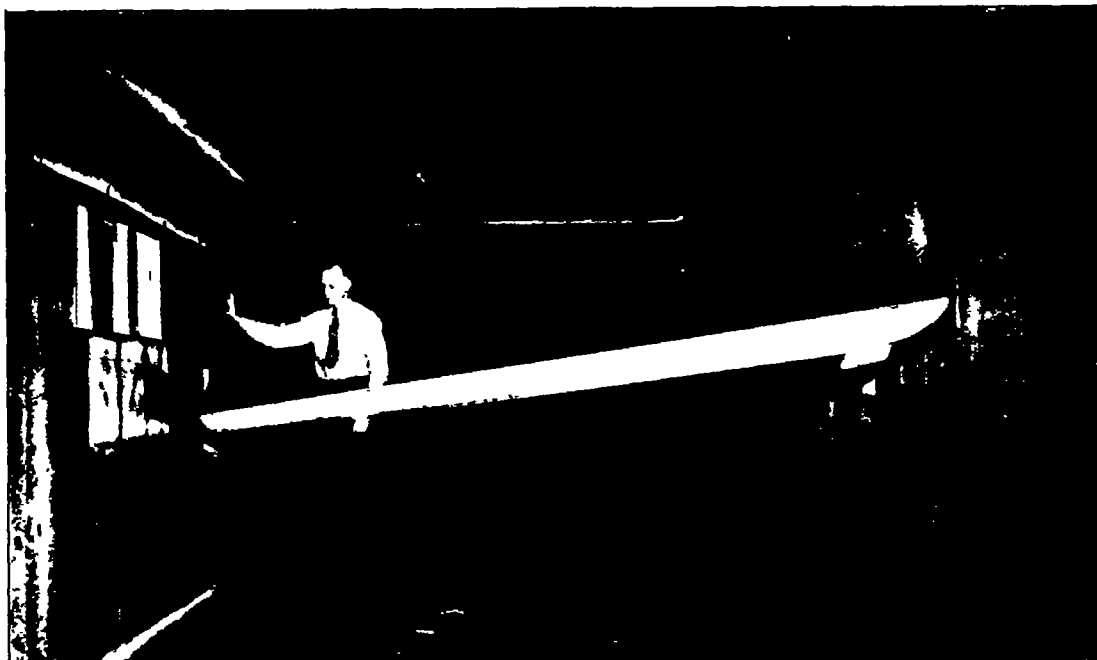
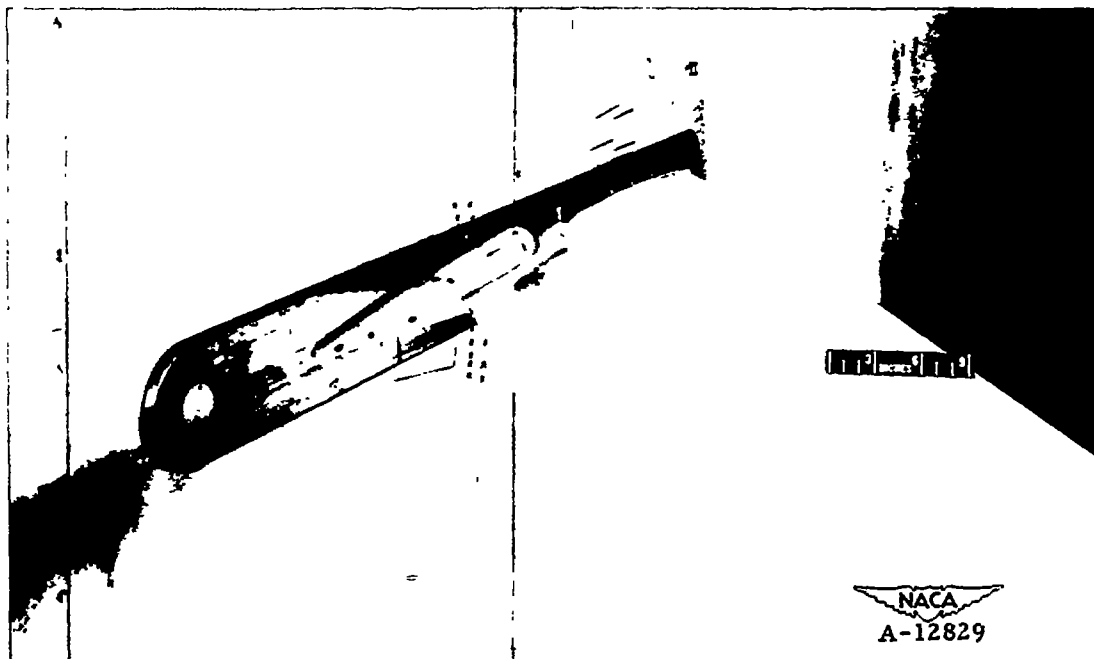


Figure 1.— Unswept wing mounted in one of the Ames 7- by 10-foot wind tunnels.





(a) Front view, positive angle of attack.



(b) Left-wall support arm showing fairing about the pressure tubes.

Figure 2.- Swept wing.





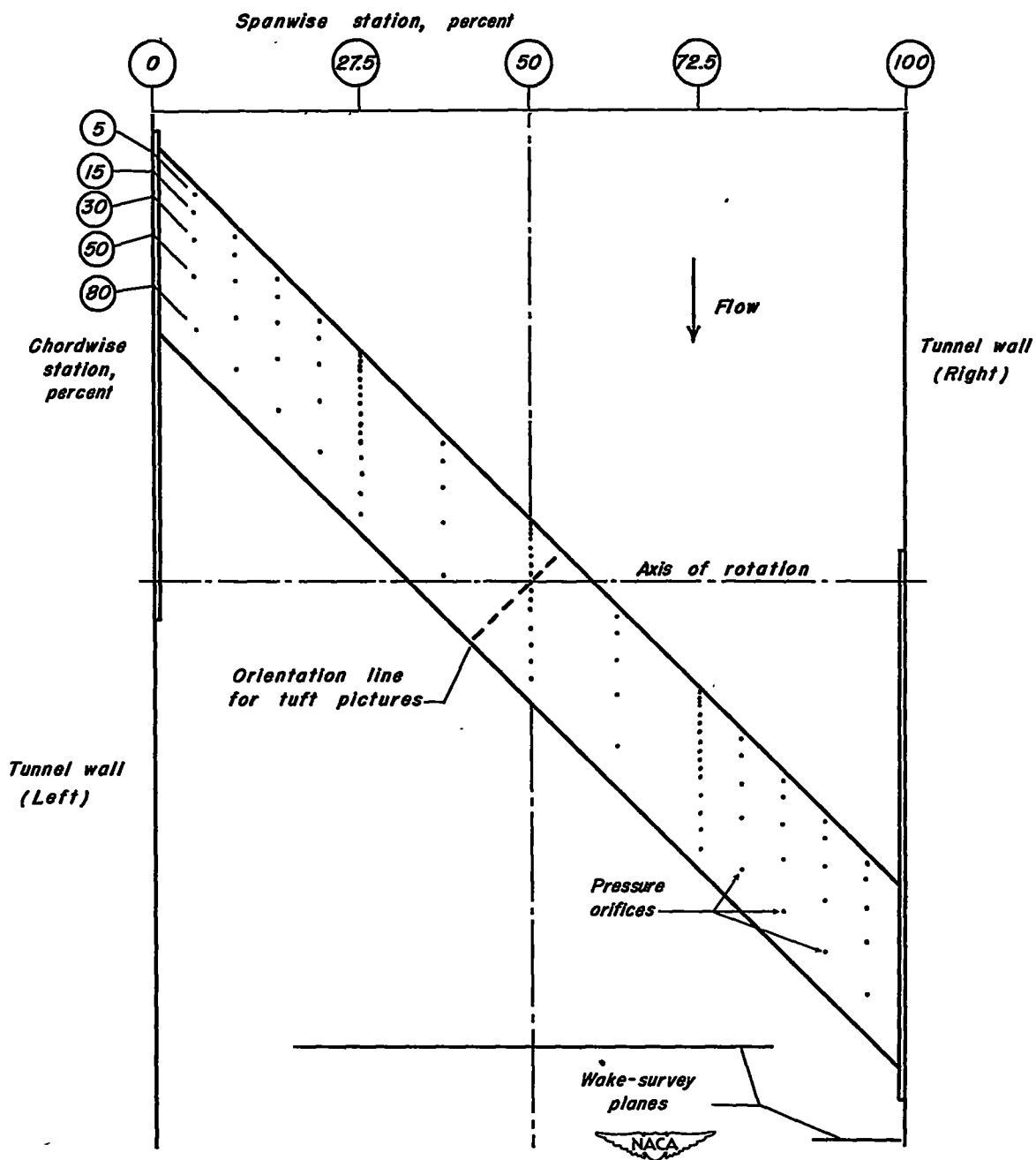


Figure 3.— Sketch of swept wing.

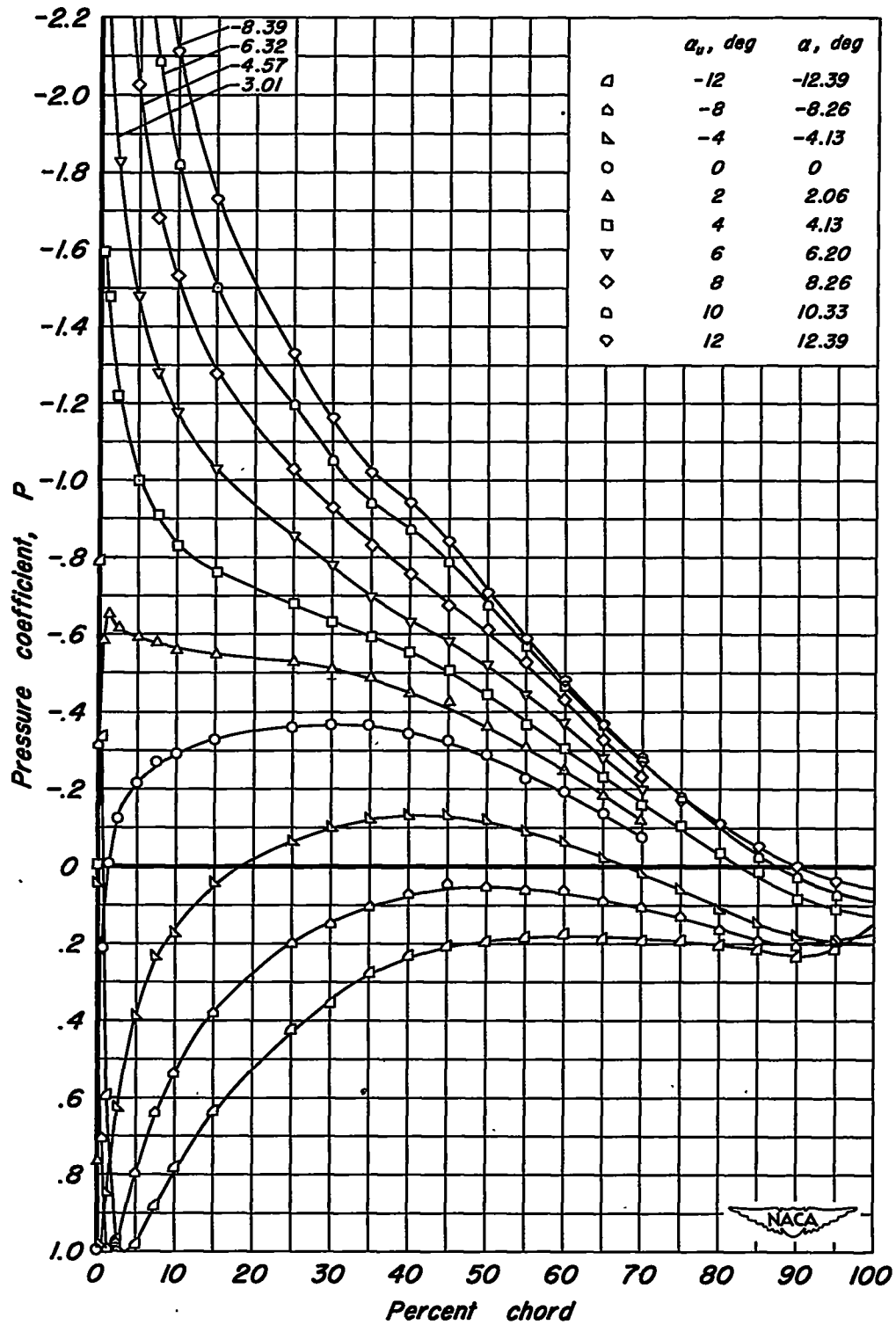


Figure 4.—Chordwise distribution of pressure over the upper surface of the unswept wing.

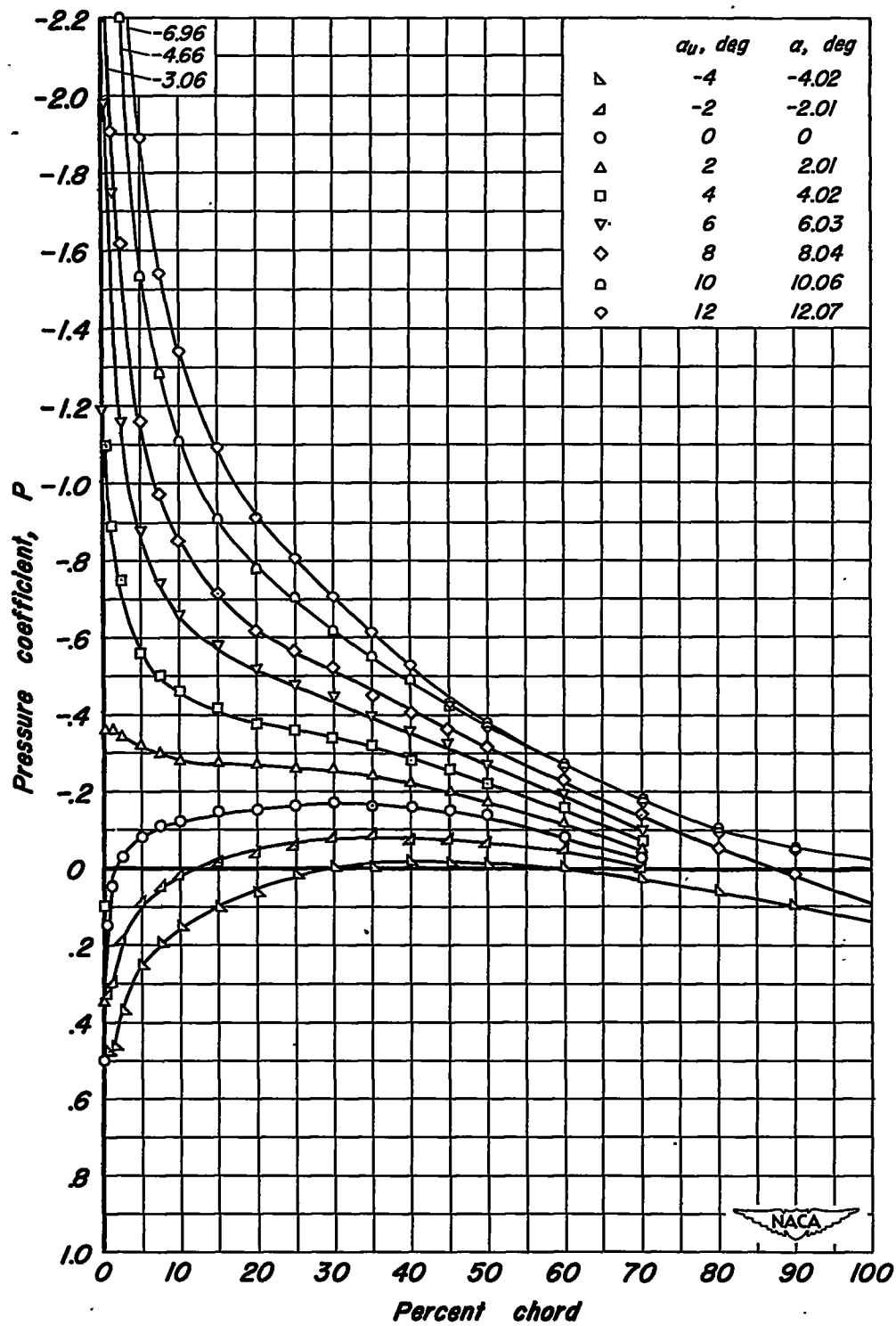


Figure 5.-Streamwise distribution of pressure over the upper surface of the swept wing.

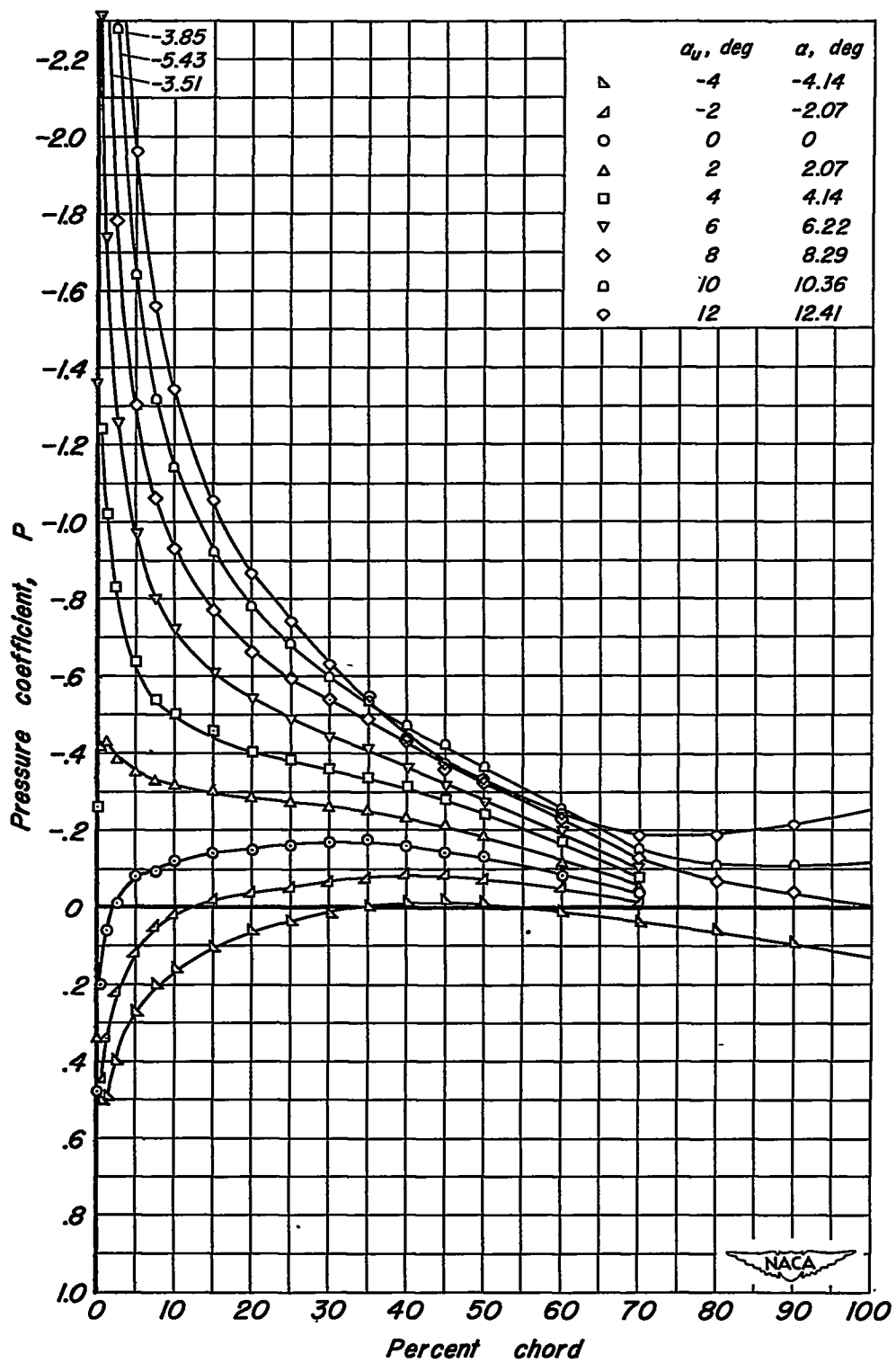
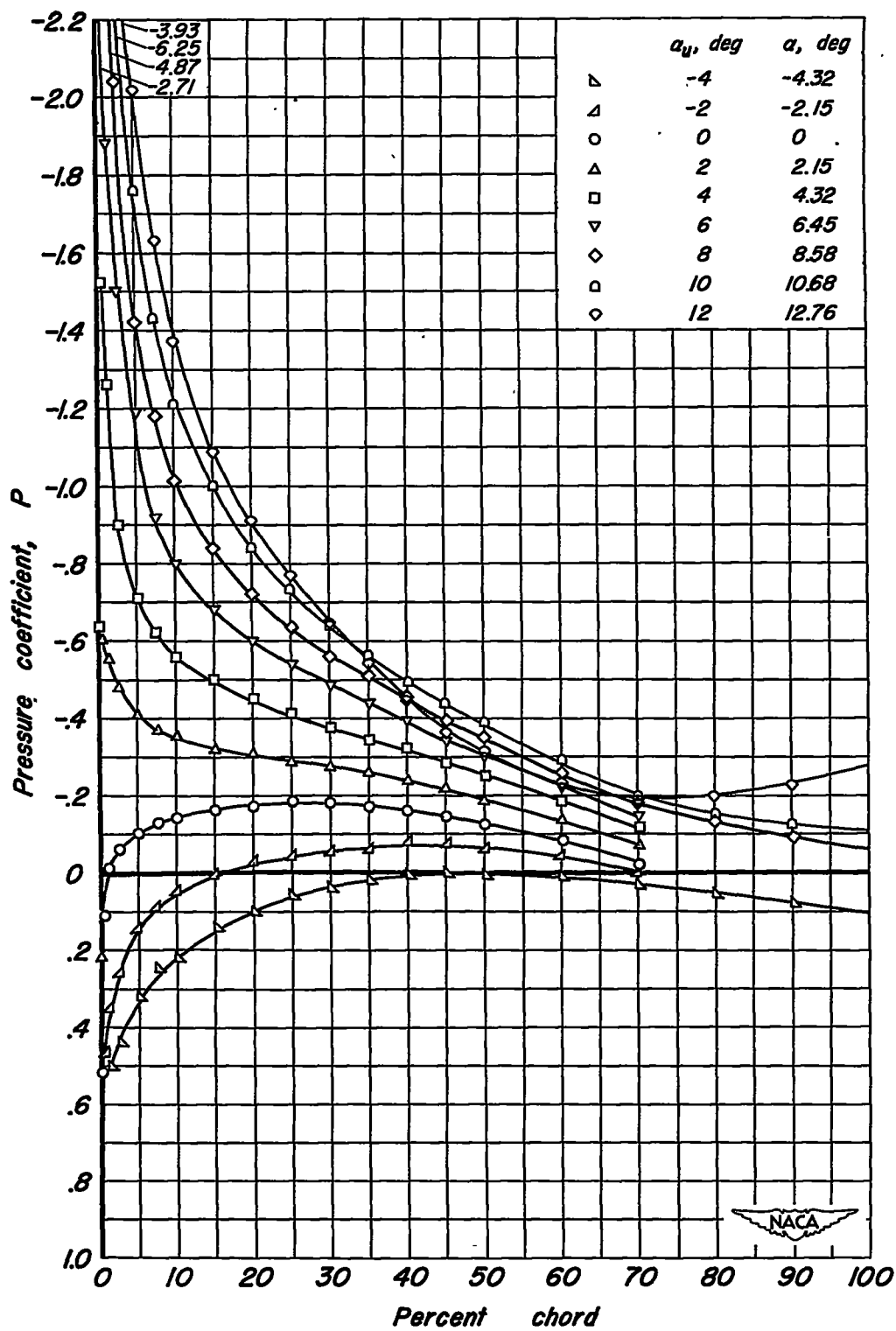


Figure 5.- Continued.



(c) Percent span station, 72.5.

Figure 5.- Concluded.

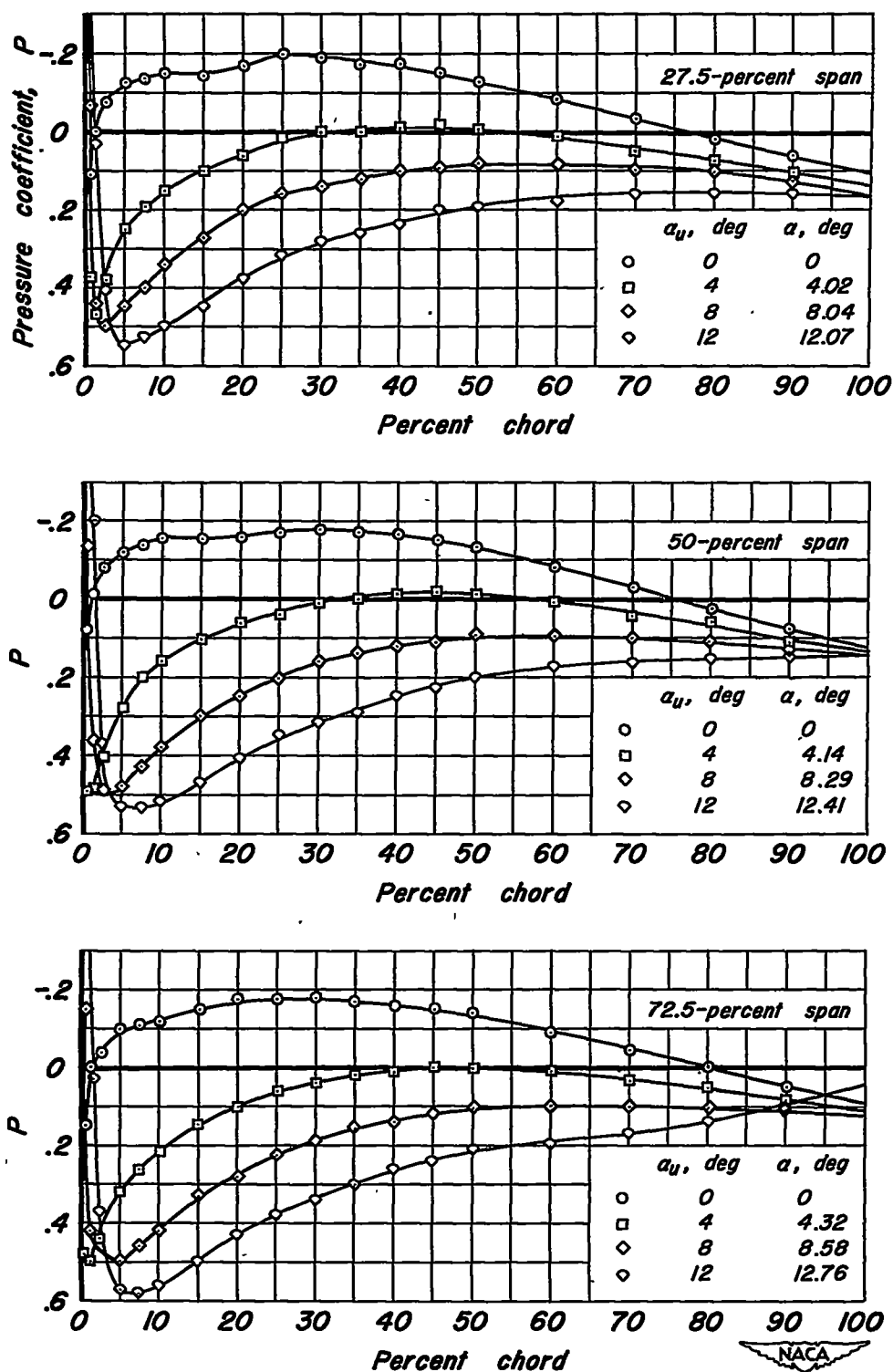


Figure 6.- Streamwise distribution of pressure over the lower surface of the swept wing.

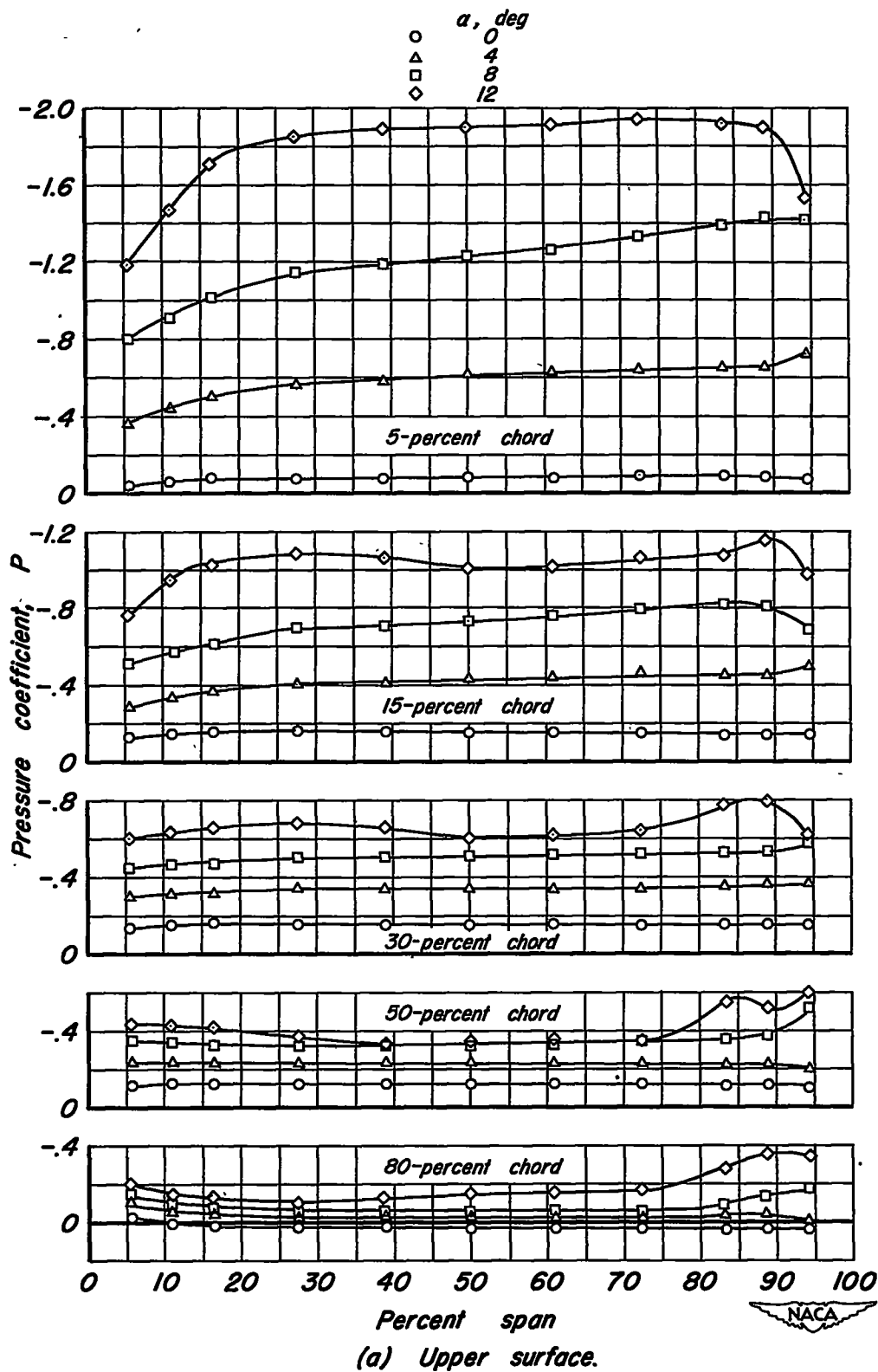


Figure 7.-Spanwise distribution of pressure over the swept wing.



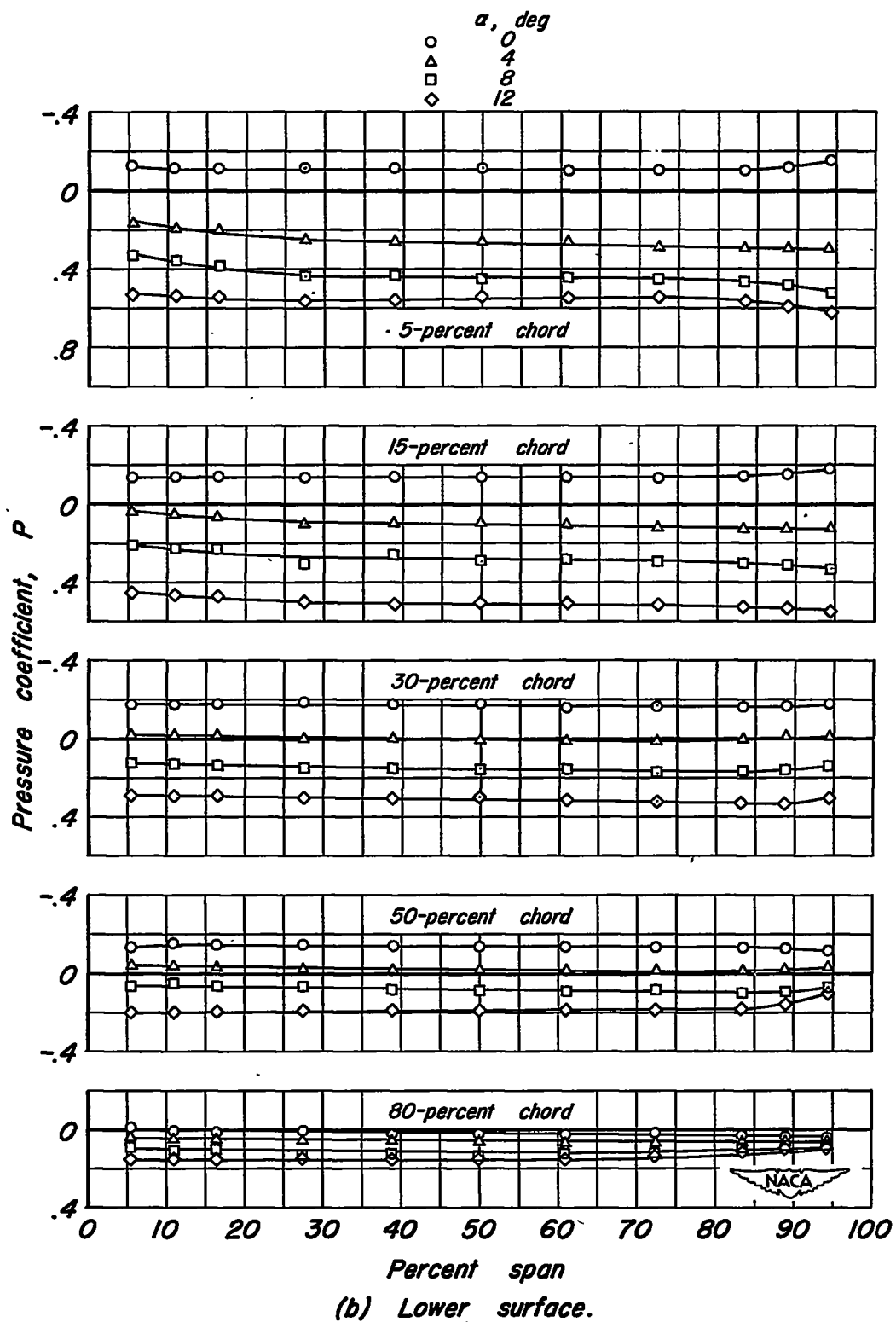


Figure 7.— Concluded.

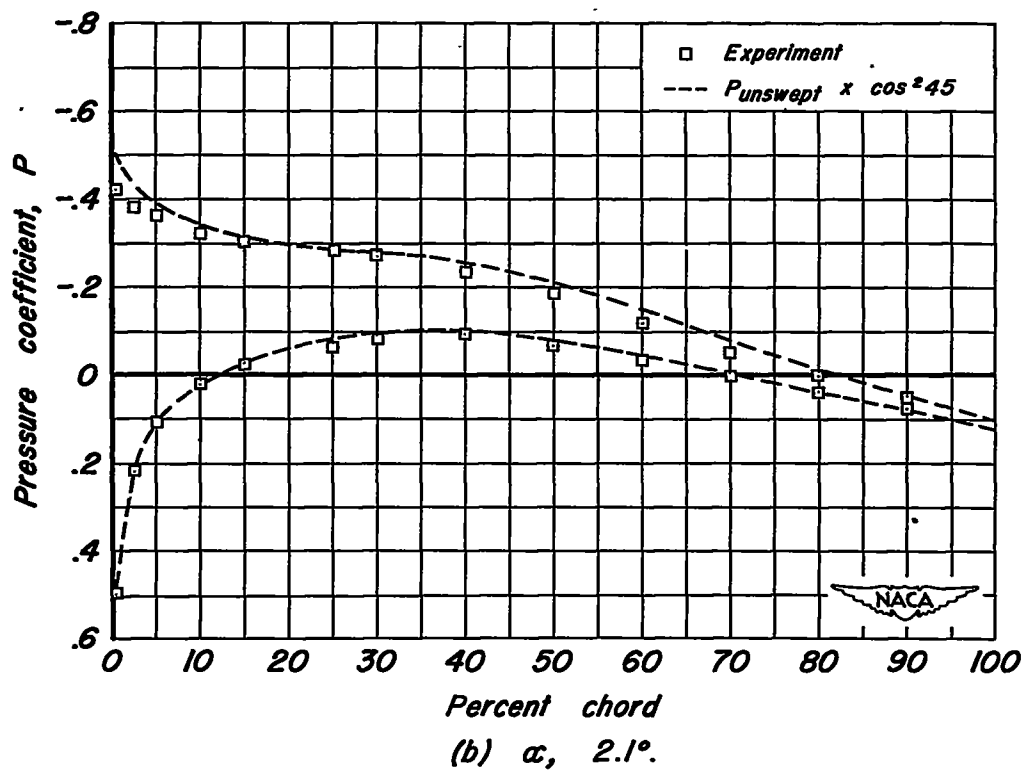
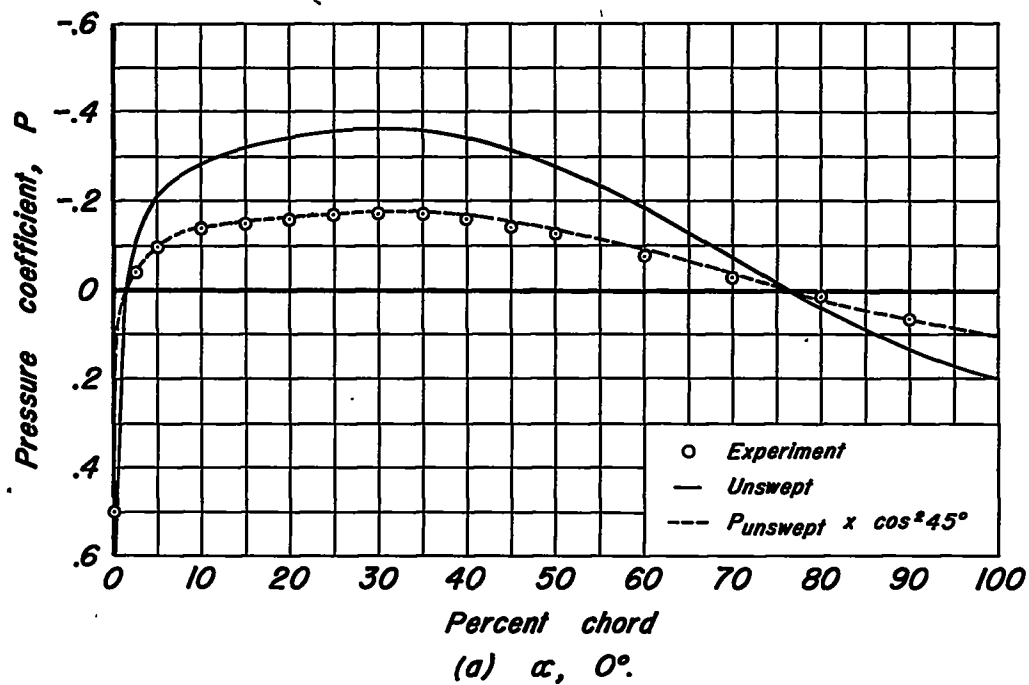


Figure 8.—Comparison of the experimental pressure distribution over the swept wing with that calculated from the unswept wing using simple sweep theory. Percent span station, 50.0.

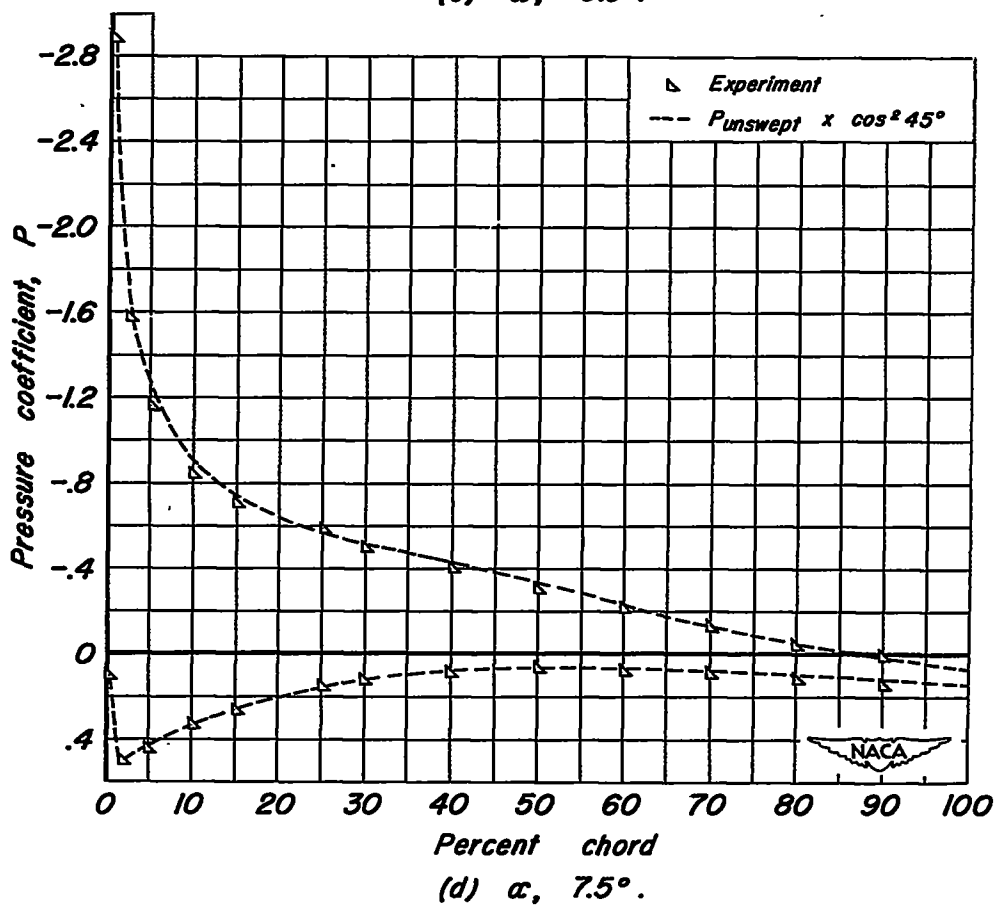
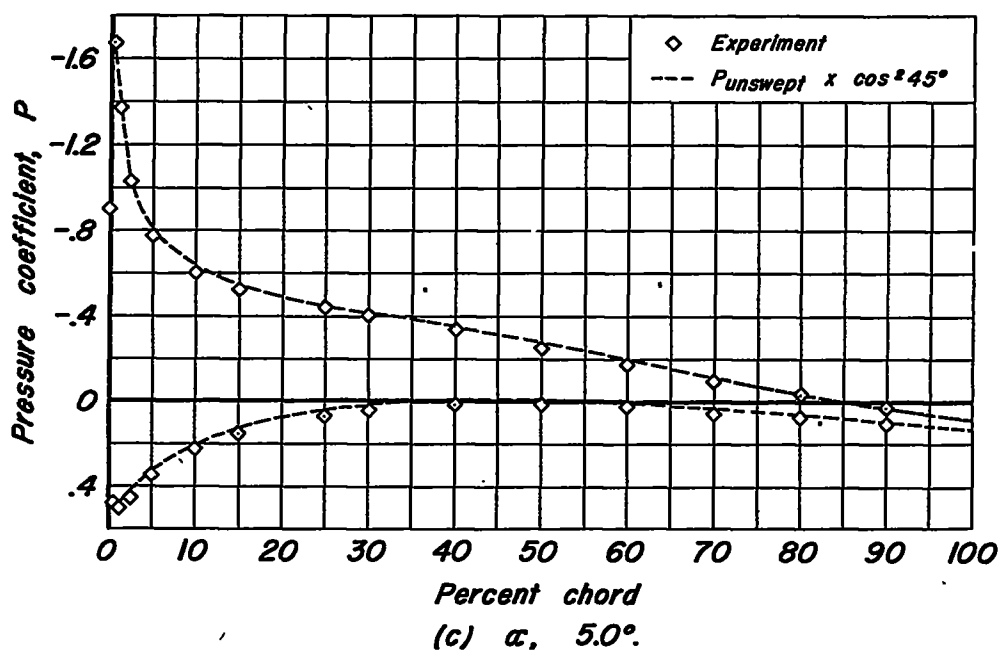


Figure 8.- Concluded.

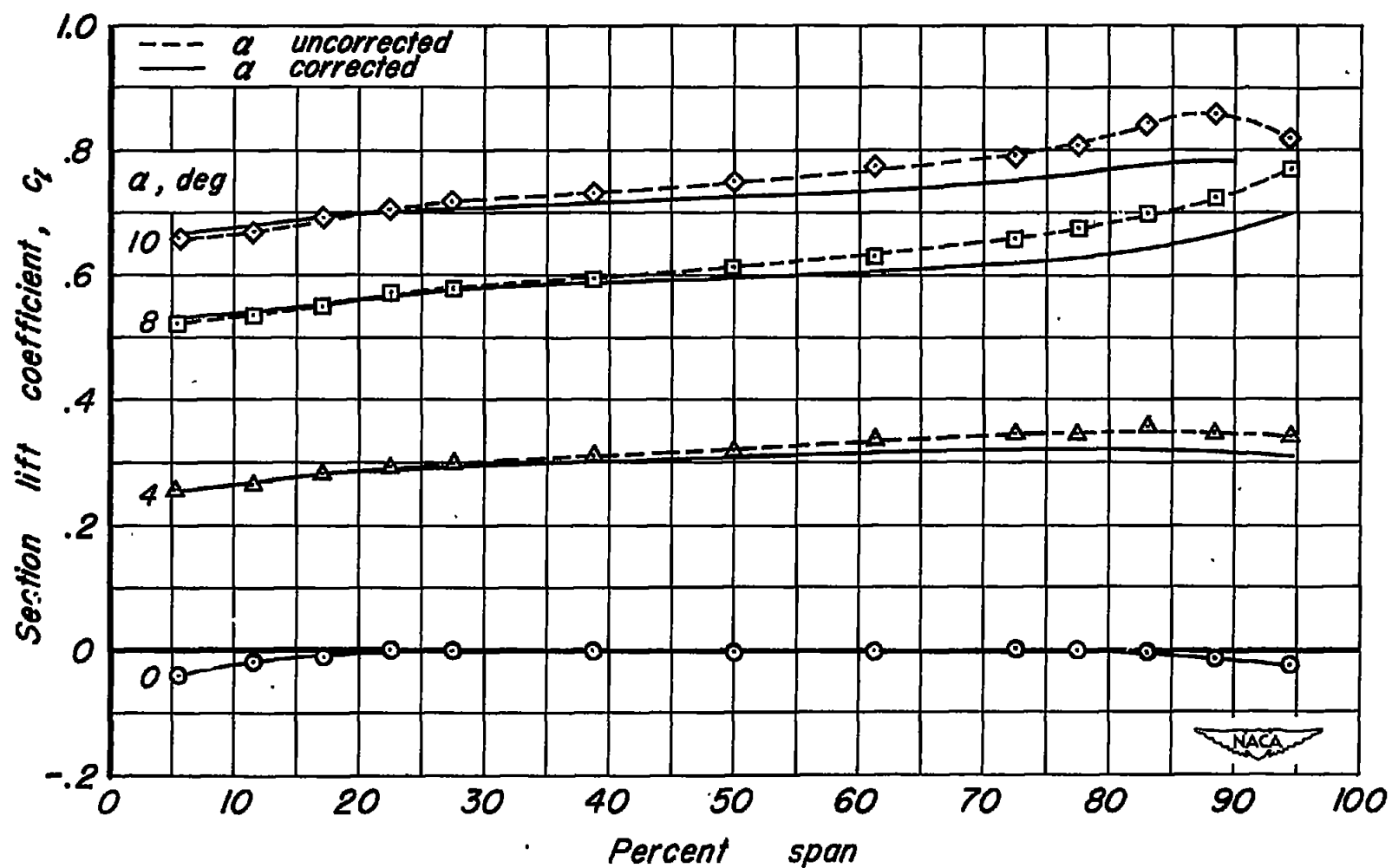
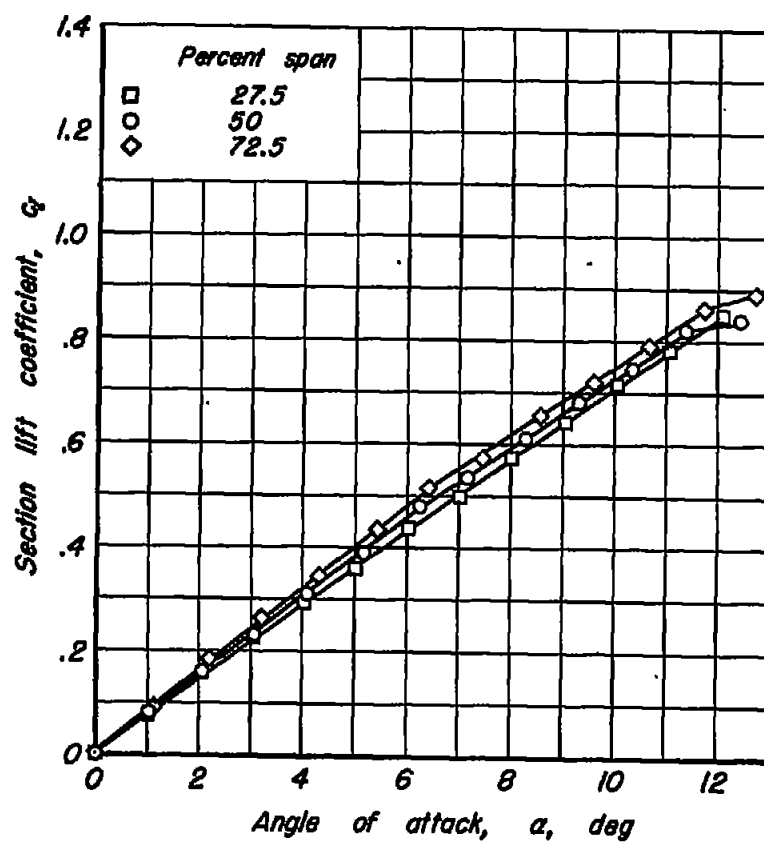
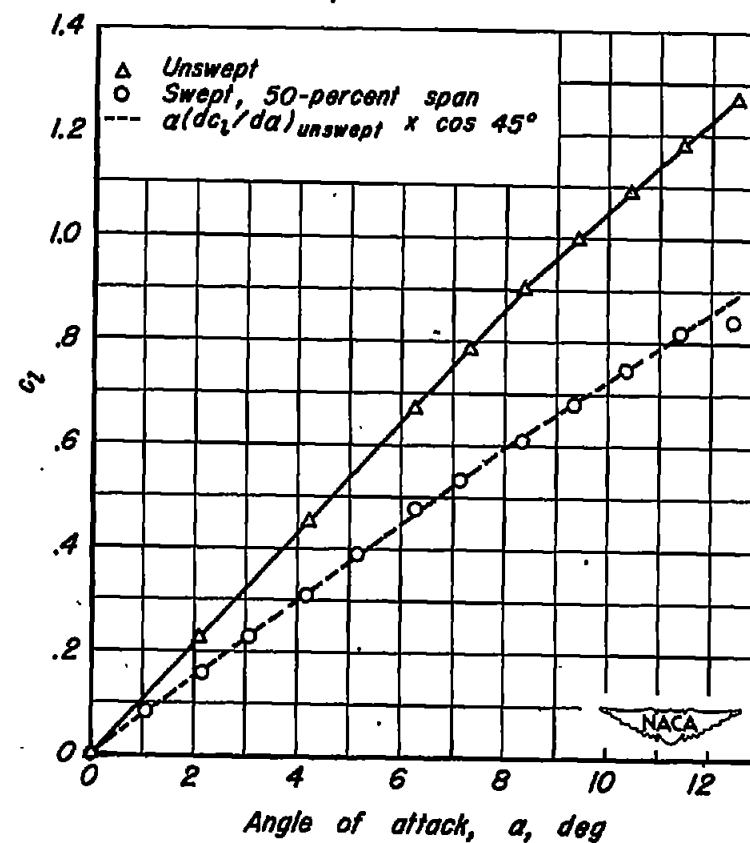


Figure 9.— Variation of section lift coefficient along the span of the swept wing.

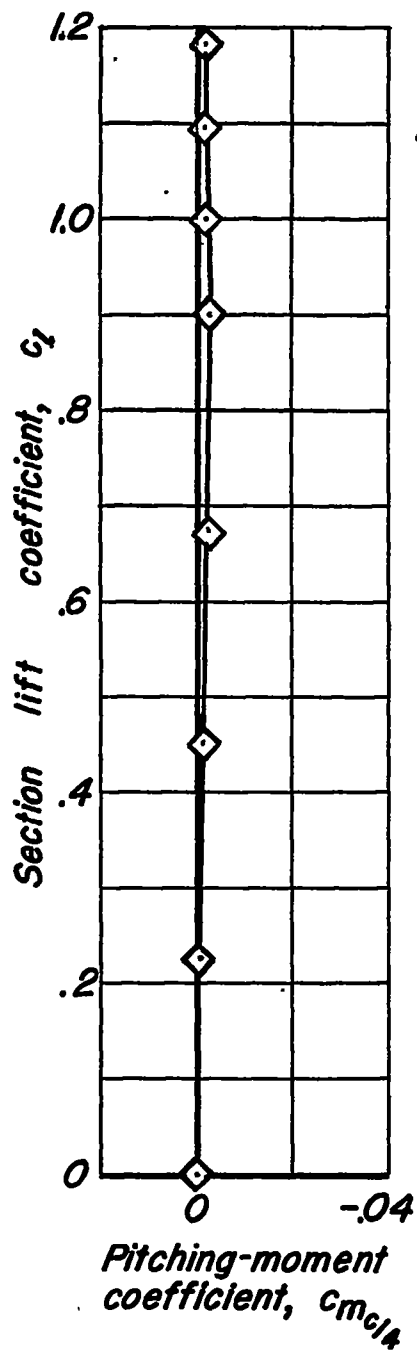
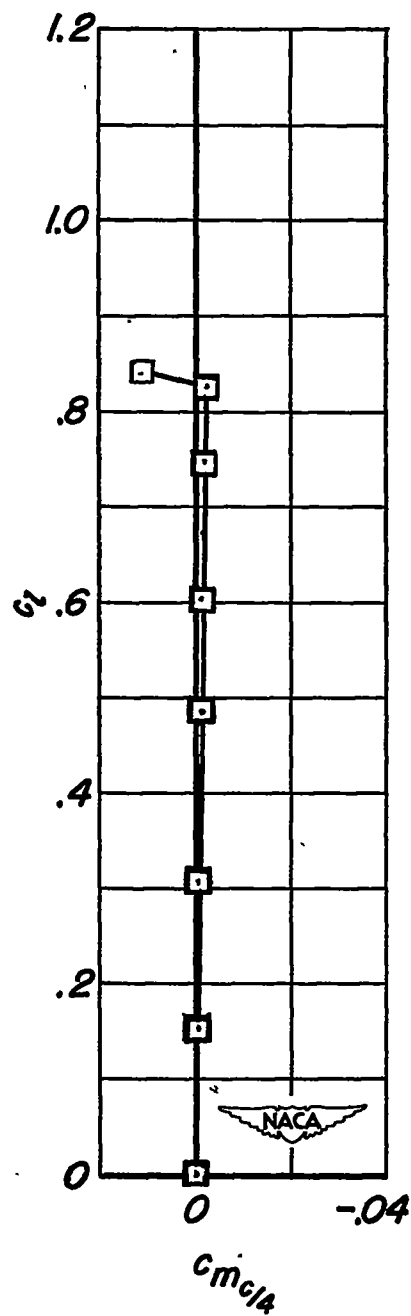


(a) Swept wing.



(b) Unswept wing and midspan station for swept wing.

Figure 10.—Section lift characteristics of the unswept and the swept wings.

*Unswept wing**Swept wing  
50-percent  
span station*

**Figure 11.— Section pitching-moment characteristics of the unswept and swept wings.**

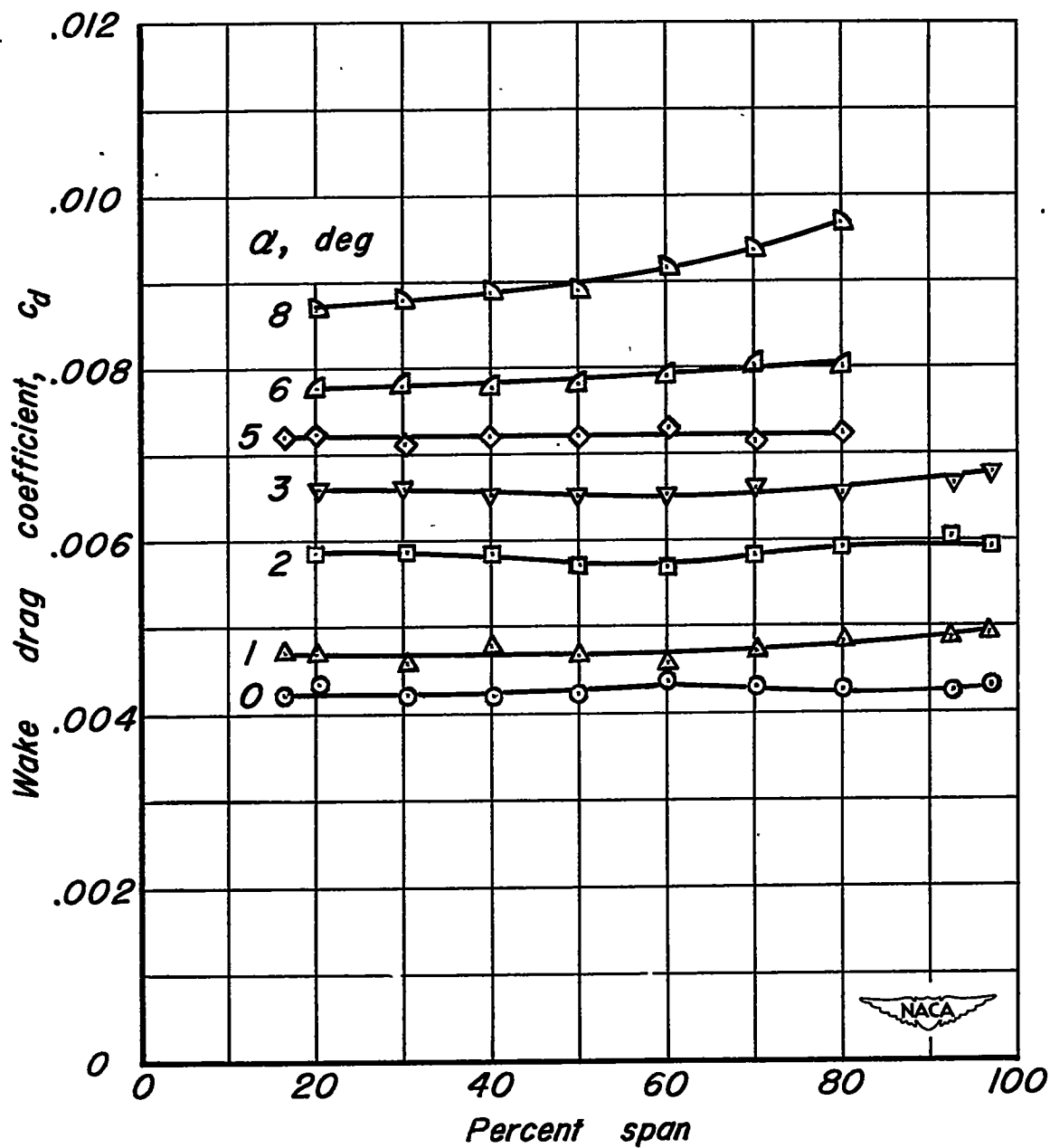
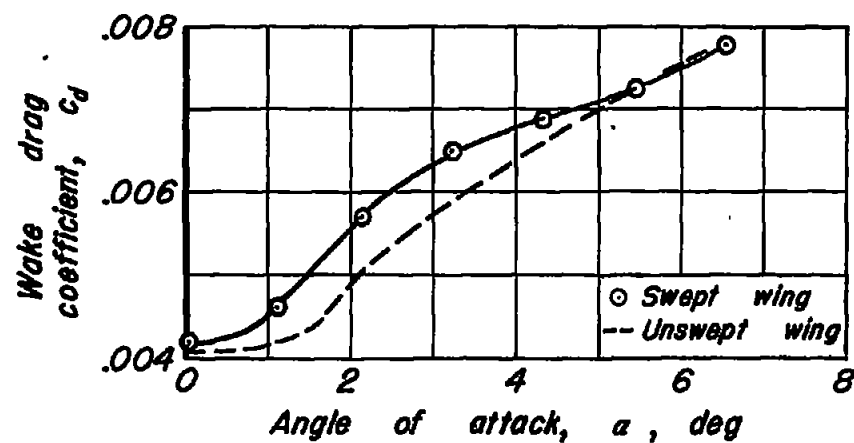
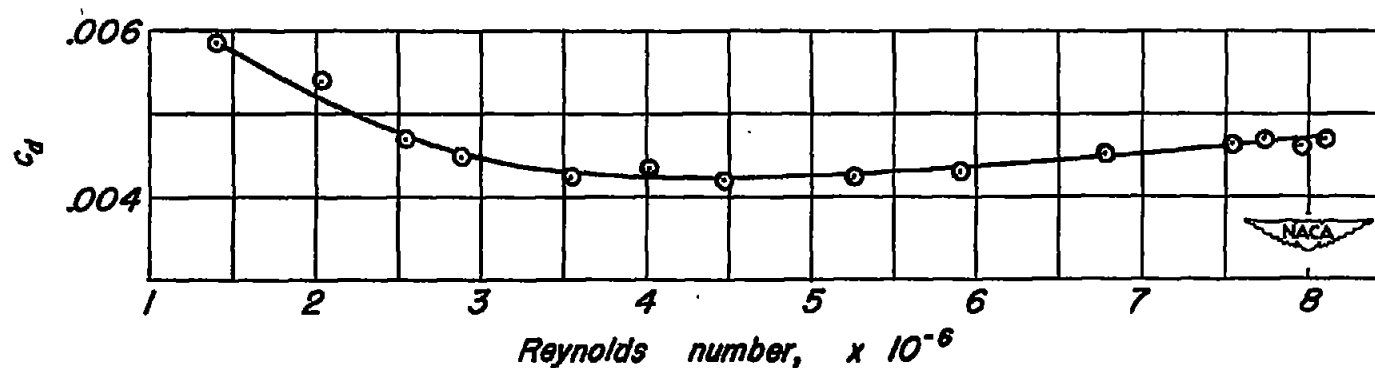


Figure 12.—Variation of the wake drag coefficient along the span of the swept wing.



(a) Variation of wake drag coefficient with angle of attack.

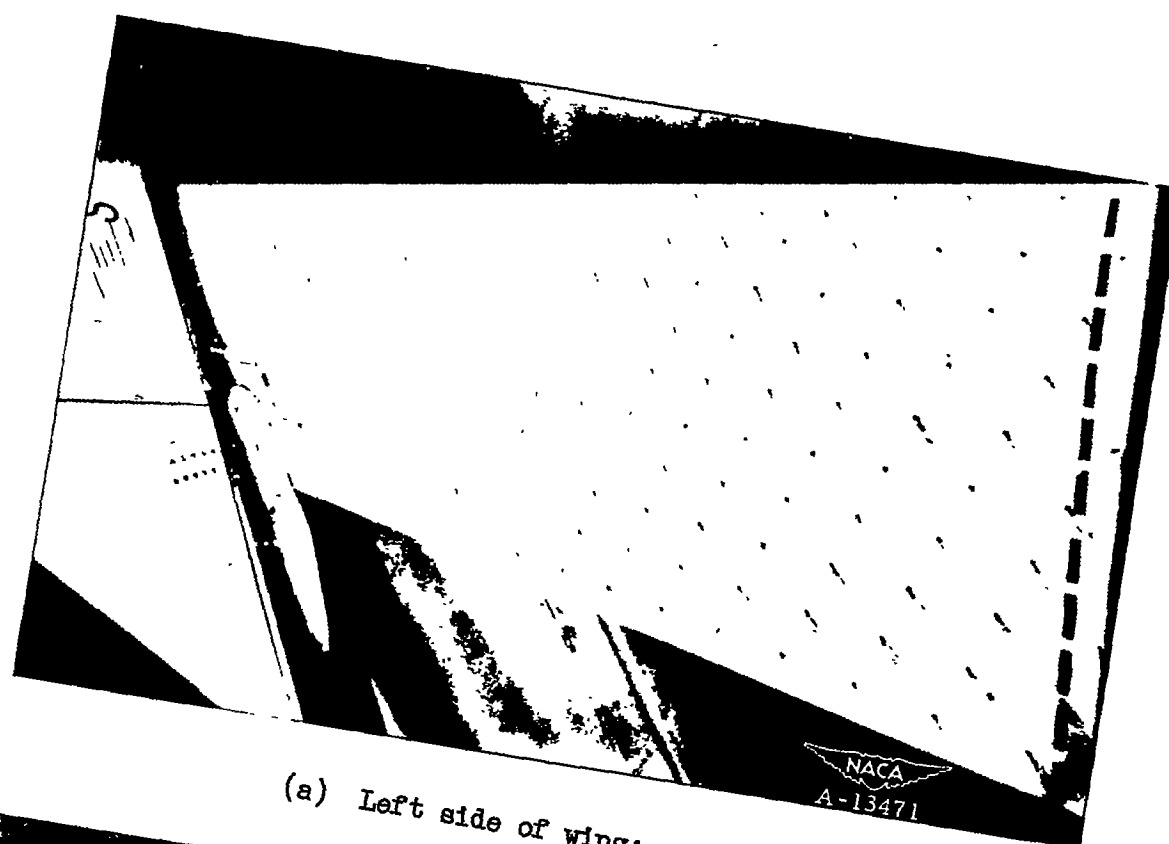


(b) Variation of wake drag coefficient of swept wing with Reynolds number.  $\alpha$ ,  $0^\circ$ .

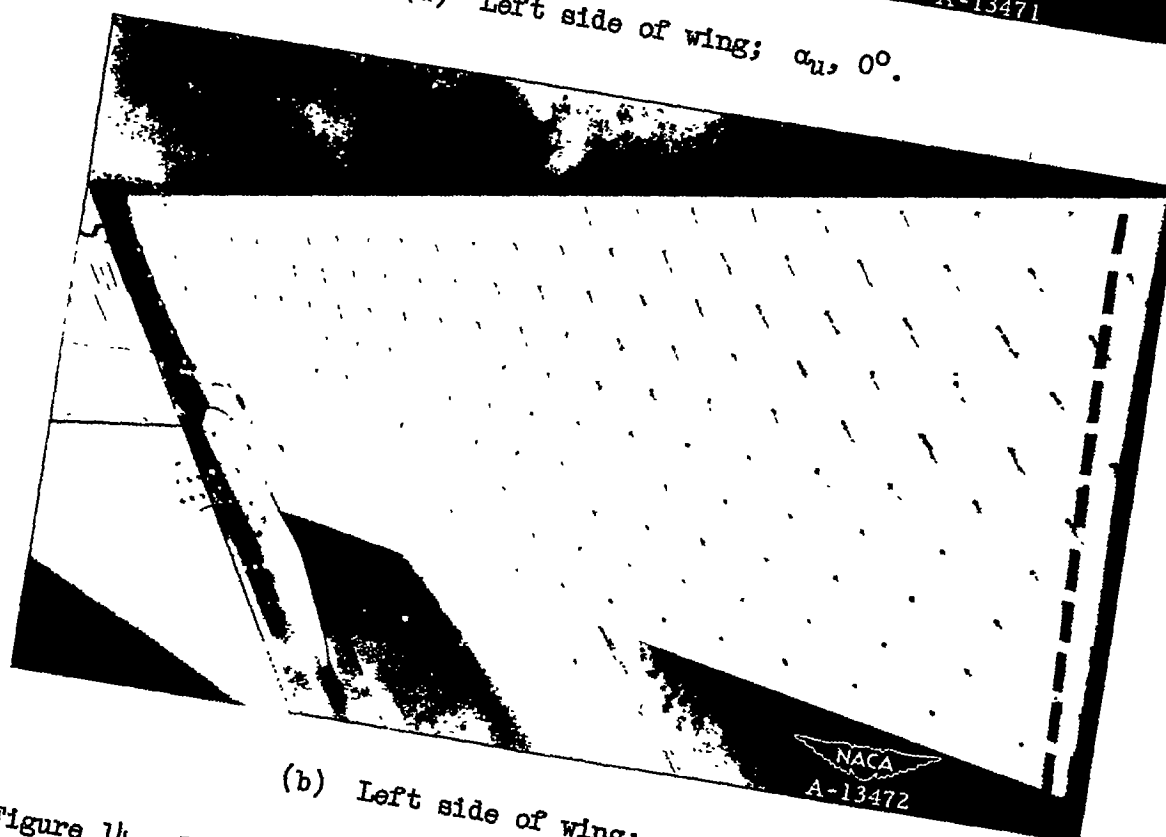
Figure 13.— Wake drag characteristics at the midspan of the swept and unswept wings.







(a) Left side of wing;  $\alpha_u, 0^\circ$ .



(b) Left side of wing;  $\alpha_u, 5^\circ$ .

Figure 14.— Tuft studies of the flow over the upper surface of the swept wing.



NACA TN 2160

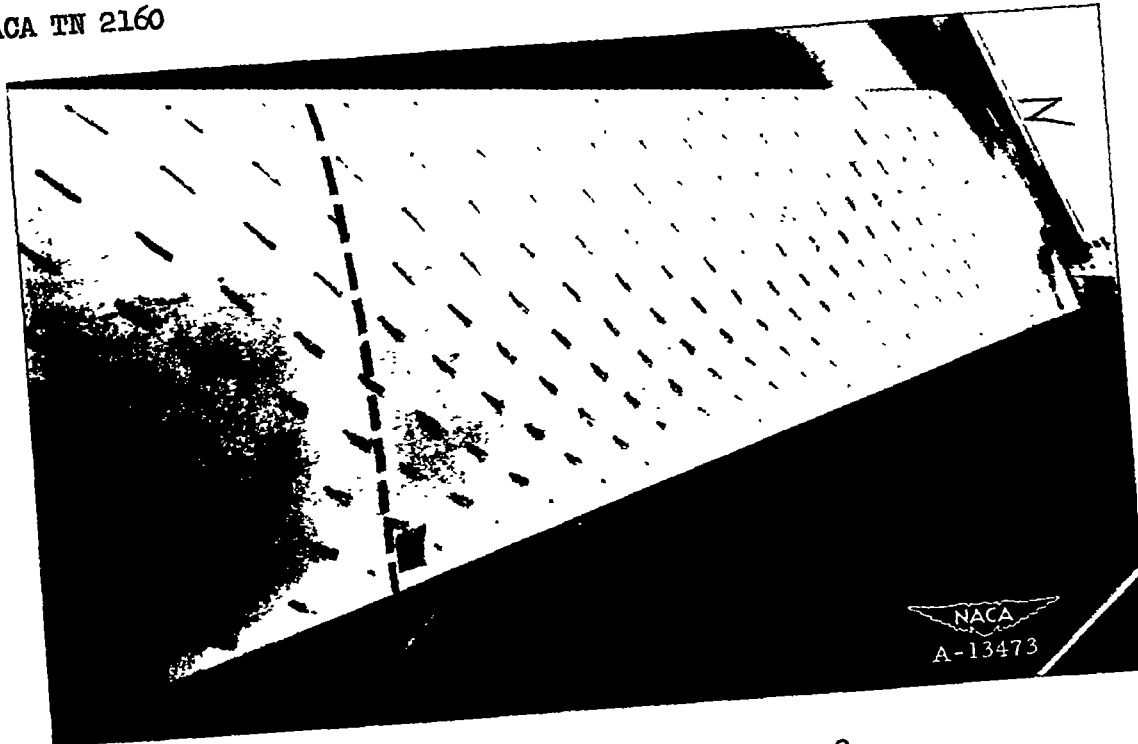
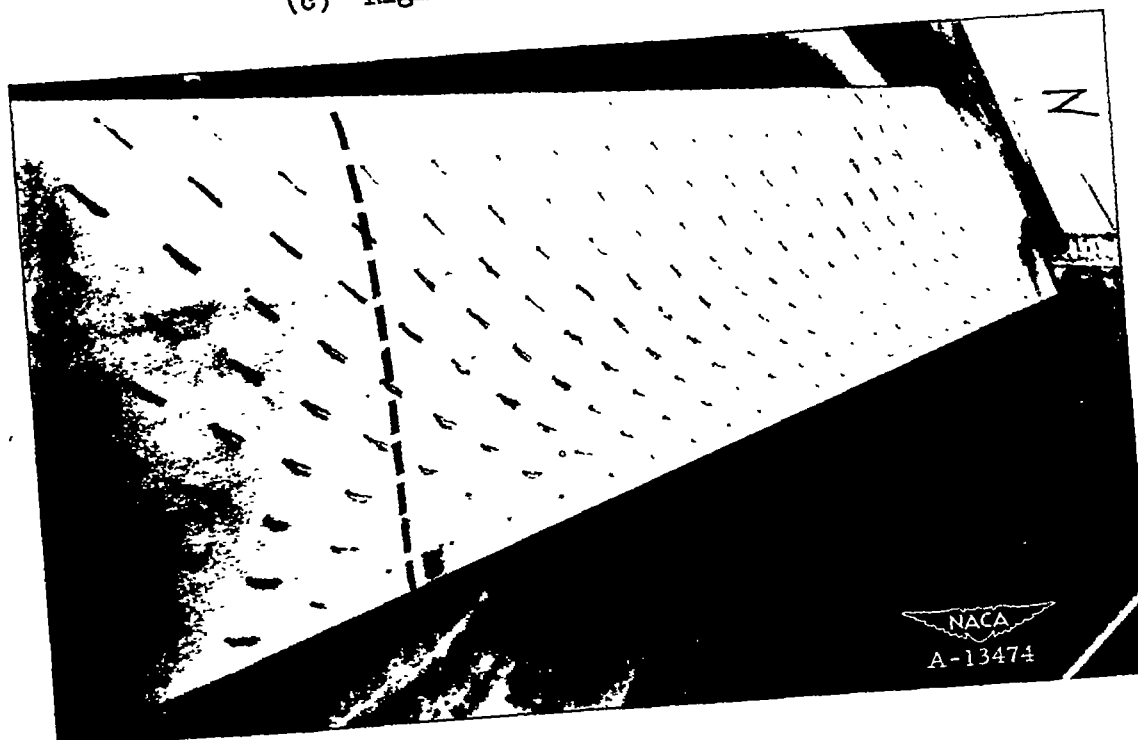
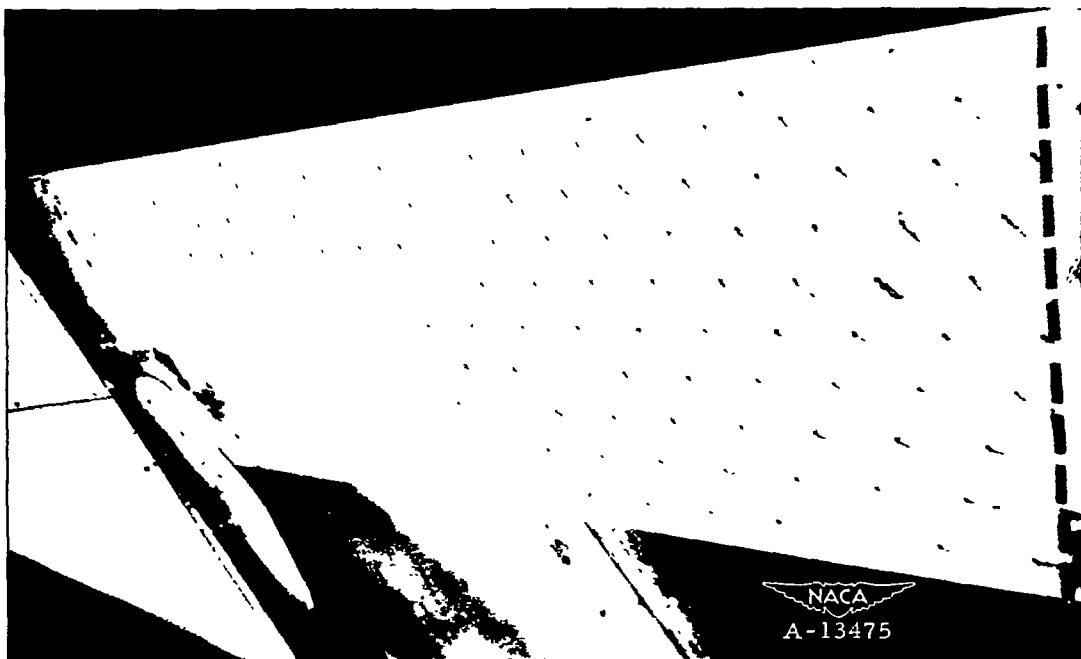
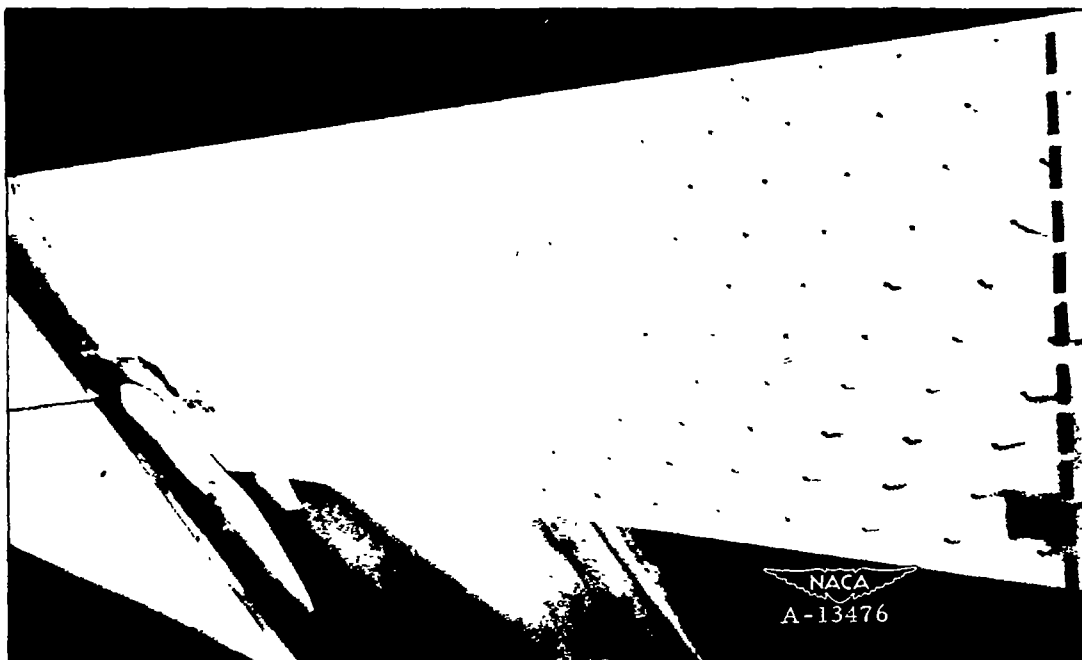
(c) Right side of wing;  $\alpha_u, 0^\circ$ .(d) Right side of wing;  $\alpha_u, 5^\circ$ .

Figure 14.- Continued.





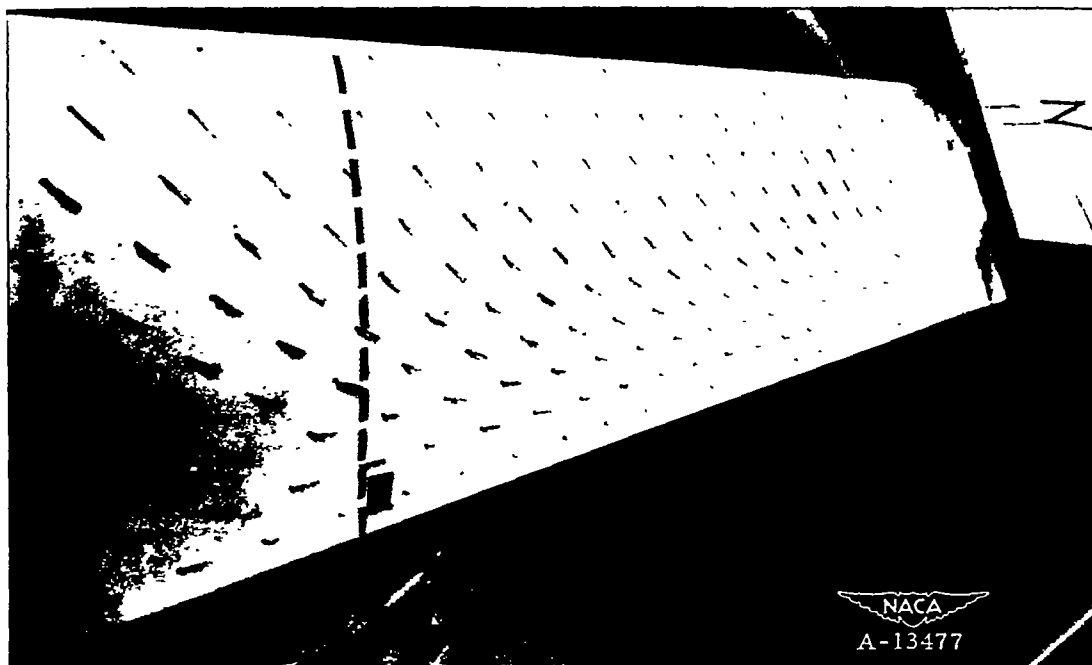
(e) Left side of wing;  $\alpha_u, 8^\circ$ .



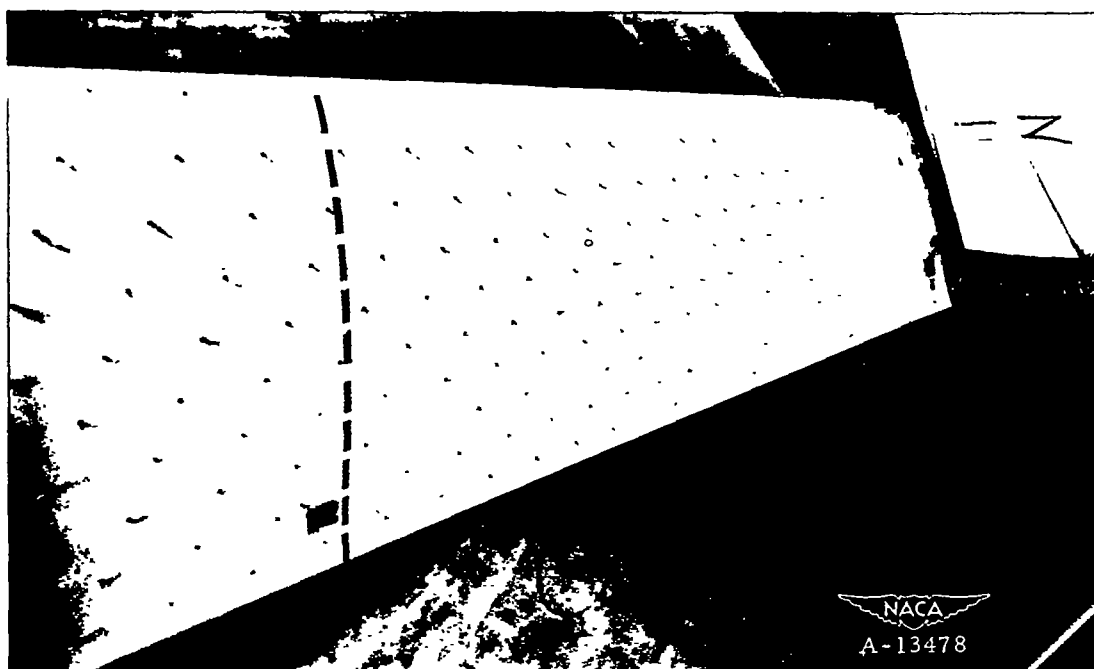
(f) Left side of wing;  $\alpha_u, 12^\circ$ .

Figure 14.- Continued.





(g) Right side of wing;  $\alpha_u, 8^\circ$ .

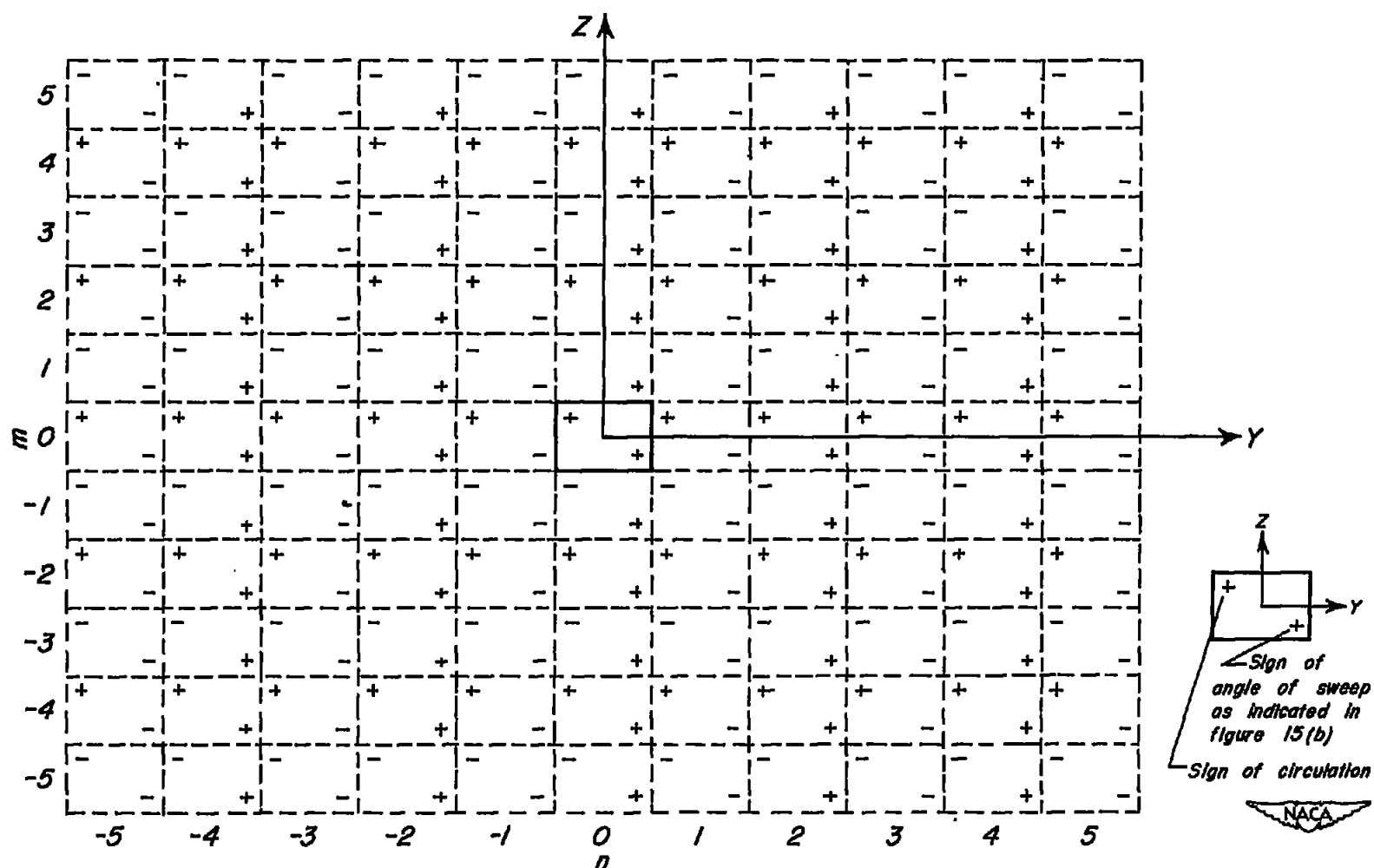


(h) Right side of wing;  $\alpha_u, 12^\circ$ .

Figure 14.- Concluded.

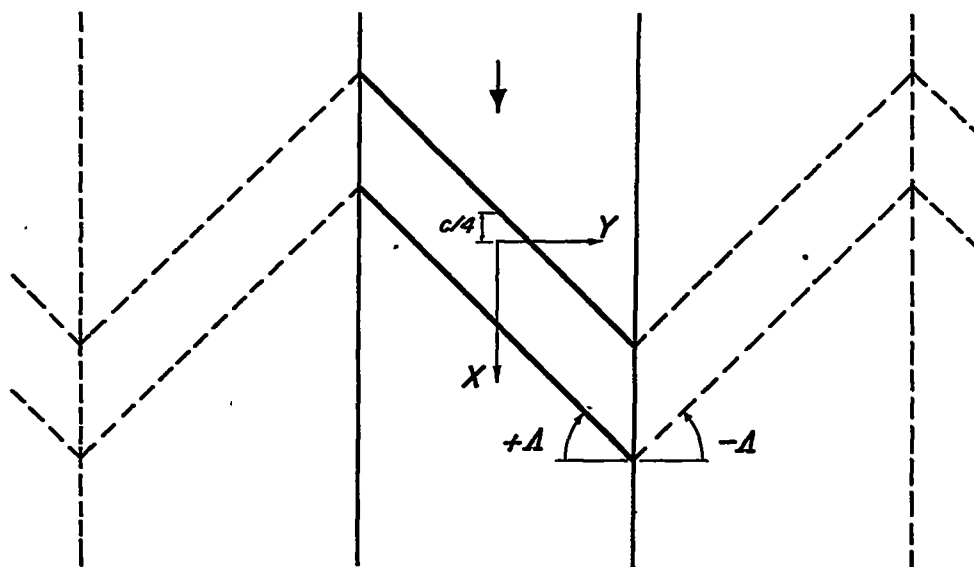




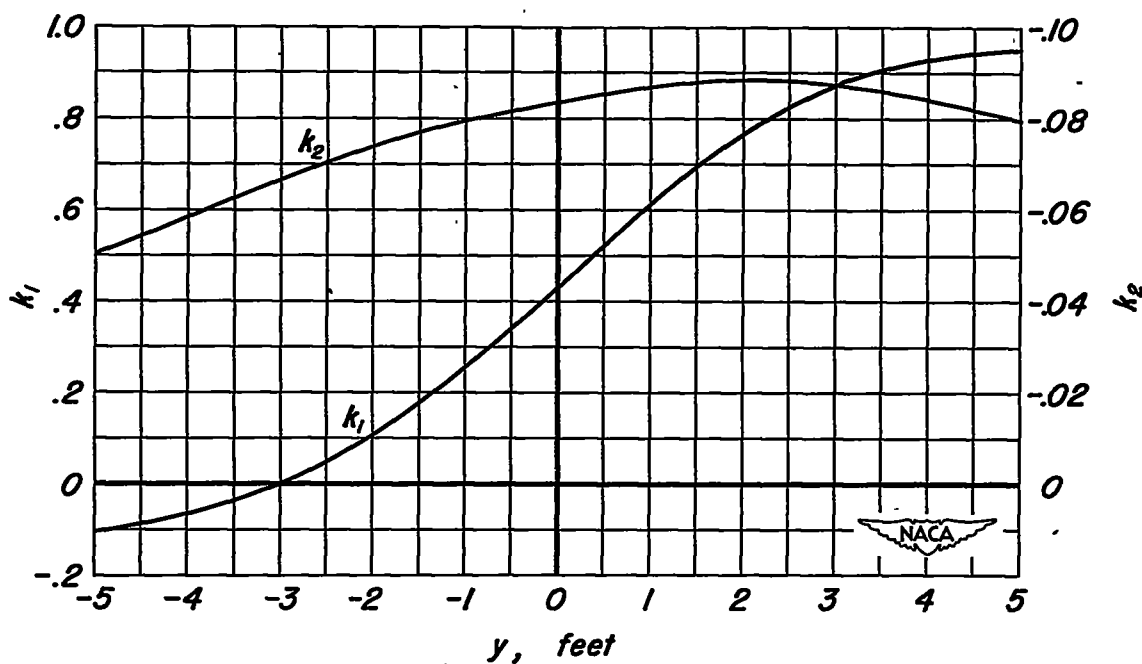


(a) Image arrangement in the  $Y-Z$  plane viewed from a position downstream.

Figure 15.- Image system and interference factors for the  $45^\circ$  swept wing mounted horizontally in a 7- by 10-foot wind tunnel.



(b) Image arrangement in the  $X$ - $Y$  plane.



(c) Variation of interference factors  $k_1$  and  $k_2$  with distance along span.

Figure 15.- Concluded.